

ATOMIC AND LASER SPECTROSCOPY

CLARENDON PRESS · OXFORD

1977

The Hanle effect and the theory of resonance fluorescence experiments

From the beginning of this century experiments using resonance radiation and resonance fluorescence have been largely responsible for our increasing understanding of excited atoms and their interaction with radiation. In the 1920's the polarization of resonance fluorescence from atoms subjected to external magnetic fields was studied in detail by Hanle and used to measure radiative atomic lifetimes.

More recently Brossel and Kastler (1949) and Kastler (1950) pointed out that polarized resonance radiation could be used to produce and detect differences in the populations of the Zeeman sub-states of both excited and ground state atoms. Following these suggestions, the techniques of magnetic resonance were widely applied to a study of bulk samples of free atoms. These experiments enabled detailed information about the Zeeman and hyperfine structure of excited and ground levels of atoms to be obtained, together with measurements of radiative lifetimes and interatomic collisional relaxation rates. The techniques of magnetic depolarization by resonance fluorescence, magnetic-optical double-resonance, and optical pumping of metastable and ground-state atoms now cover an important area in the field of atomic physics and will be discussed in this and the two subsequent chapters.

This chapter opens with an account of resonance fluorescence and its depolarization by external magnetic fields, a phenomenon now known as the Hanle effect. Experiments of this type in mercury vapour are described and we develop a classical theory to explain the shape of the observed signals. This is followed by a discussion of the applications of this technique to the accurate measurement of atomic lifetimes. For the sake of simplicity the effects of interatomic collisions and of trapping or reabsorption of resonance radiation in these experiments are not considered.

until sections 16.4 and 16.5.

Next we proceed to develop the theory of resonance fluorescence experiments using the ensemble density matrix to describe the system of atoms. The important concepts of optical and radio-frequency coherence and of the interference of atomic states are discussed in detail. As an illustration of this theory general expressions describing the Hanle effect experiments are obtained. These are evaluated in detail for the frequently employed example of atoms whose angular momentum quantum numbers in the ground and excited levels are $J_g=0$ and $J_e=1$ respectively. Finally resonance fluorescence experiments using pulsed or modulated excitation are described.

We stress the fact that in this chapter we are concerned only with the low field Zeeman effect of the even isotopes of an element. This simplification is not fundamental and is made purely for the sake of clarity of exposition. The effects of hyperfine structure in the odd isotopes and of the decoupling of the electronic and nuclear spins which occurs in large magnetic fields will be considered in Chapter 18.

15.1. Resonance radiation and resonance fluorescence

The simple spectra of many elements are dominated by one or two lines of enormous intensity, the most familiar example being the intense yellow emission from the sodium lamps used in street lighting. These transitions, which in sodium occur at 5896 \AA and 5890 \AA , are known as the *resonance lines* of the given element and often have absorption oscillator strengths close to unity. Generally they are the spectral lines of longest wavelength connecting the excited levels with the ground state by means of allowed electric dipole transitions.

When the yellow light from a sodium lamp is focussed into an evacuated cell containing sodium vapour in equilibrium with the metal, only a little stray light due to reflection will be seen when the cell is cold. However, at

temperatures of the order of 100°C a faint cone of scattered light becomes visible in the body of the cell, especially if the cell is viewed at right-angles to the incident beam. The scattered light observed in this experiment is known as *resonance fluorescence* and was first studied in detail by Wood (1913). As the cell temperature is increased still further the resonance fluorescence rapidly becomes stronger but the edges of the cone of light become increasingly diffuse owing to multiple scattering, until at 200°C the whole bulb begins to glow with resonance radiation. At very high vapour pressures the resonance fluorescence is concentrated in a thin layer close to the front face of the cell and at temperatures above 500°C , specular reflection of the incident light occurs.

This phenomenon can be easily explained in terms of the classical theory: the incident radiation sets up dipole oscillations in the medium which re-radiate electromagnetic waves of the same frequency. Resonance fluorescence is thus a special case of the scattering of light in which the frequency of the incident electromagnetic wave coincides with the natural frequency of the internal vibrations of the atomic electrons. Both the classical and quantum theory of light scattering are described in detail by Loudon (1973). However, for many of the experiments discussed in this and the two subsequent chapters, the scattering process can be considered to consist of the two separate events of excitation and radiative decay. In our present example we would say that sodium atoms in the ground level $3^2S_{1/2}$ absorb photons from the beam of resonance radiation and are raised to either of the $3^2P_{1/2,3/2}$ levels. The excited atoms in these levels have a mean lifetime of $\approx 1.6 \times 10^{-8} \text{ s}$ and then decay spontaneously, re-radiating the yellow fluorescent light in all directions.

Resonance fluorescence can be excited in the vapour of many other elements provided that suitable light sources and resonance cells are available. The equipment required in the case of mercury vapour is particularly simple and is

shown schematically in Fig. 15.1. Mercury has the advantage that a suitable vapour pressure, $\approx 1.2 \times 10^{-3}$ Torr, is obtained at room temperature and, in contrast to sodium, it

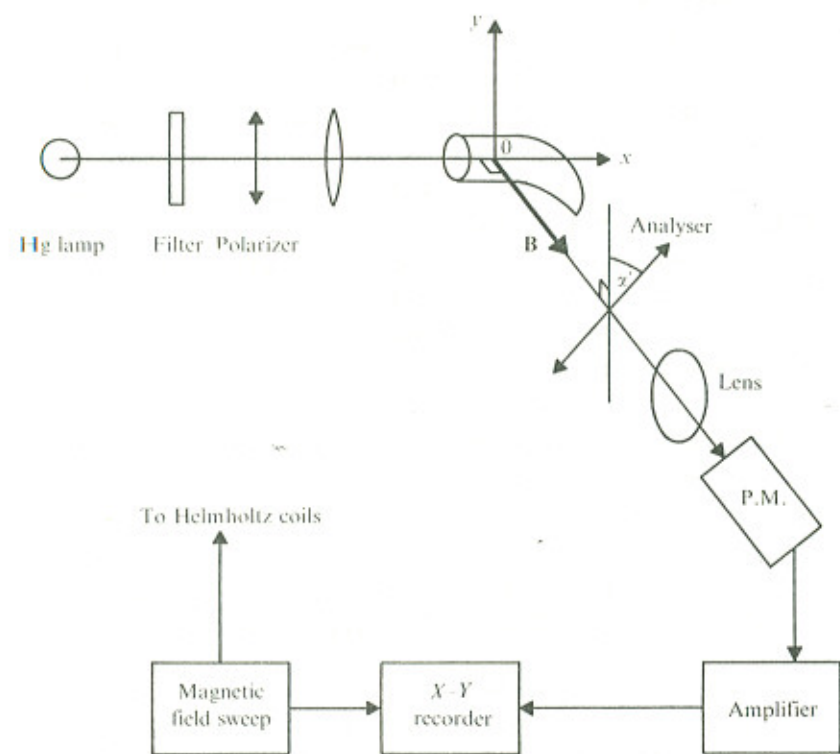


Fig. 15.1. Schematic diagram of the apparatus used for resonance fluorescence and Hanle effect experiments on the 3P_1 level of mercury.

does not react with Pyrex or quartz. Of more fundamental importance is the fact that natural mercury consists of 70 per cent of even isotopes whereas ^{23}Na has a complex hyperfine structure. The only disadvantage is that the resonance lines of mercury are in the ultraviolet, as Fig. 15.2 shows. The transition at 1850 \AA is the true resonance line but as it lies in a region where molecular oxygen is strongly absorbing,

all the optical paths in this case would have to be in vacuum or filled with nitrogen. Resonance fluorescence experiments using the intercombination line at 2537 \AA avoid this difficulty and are relatively easy to carry out. The progressive break down of L-S coupling in the heavier elements which makes this one of the most intense lines in the mercury spectrum was discussed in section 5.5.5.

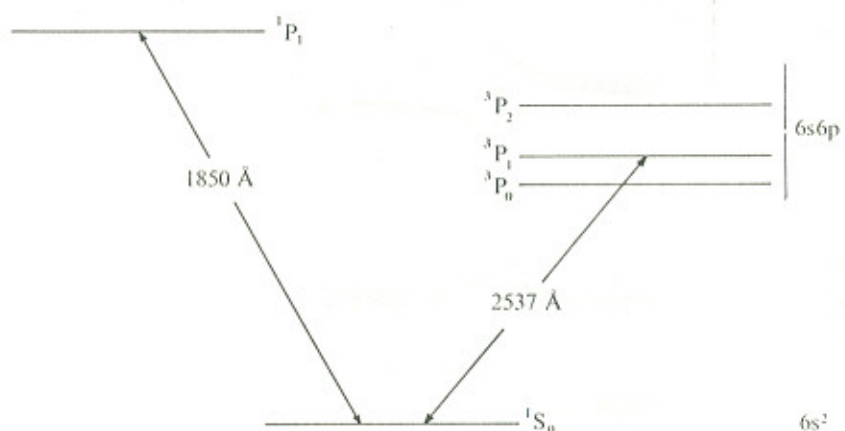


Fig. 15.2. Resonance lines and first few energy levels of mercury.

15.2. Magnetic depolarization of resonance radiation - the Hanle effect

15.2.1. Historical introduction. In one of the earliest investigations of resonance fluorescence, Lord Rayleigh (1922) showed that the radiation scattered from mercury vapour was polarized when the atoms were excited by polarized light. Soon afterwards Wood and Ellet (1924) showed that the polarization of the fluorescent light was destroyed by applying small magnetic fields to the resonance cell. Further experimental studies of this effect were made by Hanle (1924), who also worked out a classical theory describing the influence of the magnetic field on the polarization of the

resonantly scattered light. He showed that the effect, which now bears his name, could be used to measure the lifetimes of excited atoms. Interest in the field of atomic physics in general and resonance fluorescence in particular declined over the next two decades, but recently the Hanle effect has been developed into one of the most reliable methods for measuring the lifetimes of excited levels of atoms and molecules. Although we shall concentrate our attention on the alkalis and the elements of group IIB, namely Zn, Cd, and Hg, it should be remembered that this technique has been much more widely applied and experiments on the noble gases, the rare earth elements, and molecules such as NO and OH have been reported.

15.2.2. The Hanle effect in mercury. The apparatus necessary to study the magnetic depolarization of resonance radiation in mercury vapour is shown schematically in Fig. 15.1. Light from a quartz mercury lamp is passed through a filter which removes all but the 2537 \AA line and then through a linear polarizer whose transmission axis is at right angles to the direction of the magnetic field B . This field is produced in a Helmholtz coil pair which is not shown in the diagram. The resonance radiation is focussed by a quartz lens into a quartz cell placed at the centre of the Helmholtz coils. This resonance cell is prepared by evacuation to pressures below 10^{-7} Torr and is then sealed off after a small quantity of mercury has been distilled into it. For the present we shall assume that the cell contains only even isotopes of mercury. The atoms of the attenuated vapour in the resonance cell are excited by absorption of the linearly polarized light. As we will see in section 15.5, these excited atoms must be described by wavefunctions which are a coherent superposition of the $m_J=+1$ states belonging to the 6^3P_1 level. Nevertheless after a mean lifetime of $\tau \approx 10^{-7} \text{ s}$, the excited atoms decay spontaneously back to the ground level, re-emitting the 2537 \AA radiation.

The fluorescent light emitted in a direction at right-angles to the direction of the incident radiation is collected

by a fused silica lens, passed through a linear polarizer, and is detected by a photomultiplier. As the magnetic field is slowly varied from -5 G to $+5 \text{ G}$, the intensity of fluorescent light observed undergoes pronounced variations, displaying either a Lorentzian or dispersion shape centred at the zero-field position as shown in Fig. 15.3. The experimental signal is produced by a change in the state of polarization of the fluorescent light from almost perfect polarization at zero magnetic field to complete depolarization at

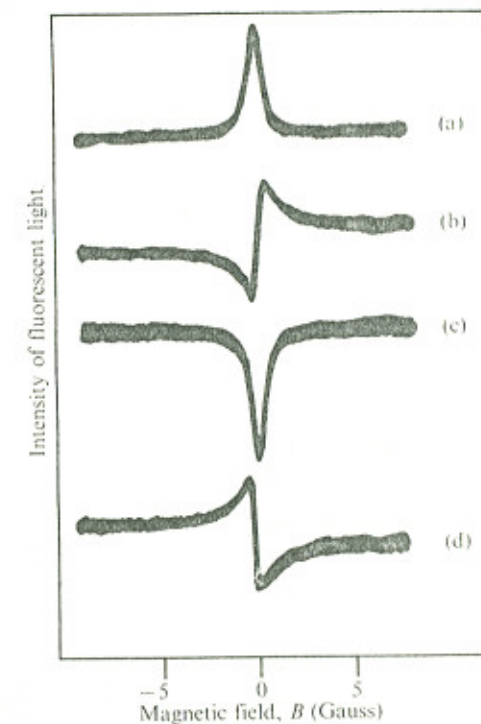


Fig. 15.3. Hanle effect or zero-field level-crossing signals for the 6^3P_1 level of mercury. The four curves correspond to rotation of the polarizer in successive steps of $\pi/4$. (After Kibble and Series (1961).)

fields of only 5-10 G. This constitutes the Hanle effect or the magnetic depolarization of resonance radiation. These experiments are also sometimes referred to as zero-field level-crossing experiments for reasons which will be explained in section 15.6.1.

15.2.3. Classical theory of the Hanle effect. The detailed dependence of the intensity of scattered light as a function of the magnetic field strength may be derived by applying the classical model in which an excited atom is represented by a single, harmonically oscillating electron. This approach is useful because it gives a clear picture of the processes responsible for the Hanle effect and correctly predicts the shape of the signals observed in all experiments. The more rigorous quantum-mechanical formulation of the theory will be considered in section 15.5 below, where it will become apparent that the Hanle effect is analogous to the perturbed angular correlations which may be observed in the γ -ray decay of excited nuclei.

The excitation process is treated by assuming that the electron in one of the atoms receives an impulse at the moment of excitation, t_0 , which starts it oscillating in a direction specified by the polarization vector of the incident radiation. This simple representation of the excitation process is valid provided that the width of the resonance line emitted by the lamp is very broad in comparison with both the natural linewidth and the Zeeman splitting of the atoms in the resonance cell. The excited electron, oscillating at the angular frequency, ω_0 , now radiates in the usual dipole distribution pattern producing an electric field at a point on the axis of observation given by

$$\underline{E}(t) = E(0) \exp\{-i(\omega_0 - i\Gamma/2)(t-t_0)\} \hat{j}. \quad (15.1)$$

For the present we assume that the damping constant is determined only by the radiative lifetime of the excited atom, $\Gamma=1/\tau$. From equation (15.1) we see that at zero magnetic field the fluorescent light is linearly polarized in a direc-

tion parallel to the electric vector of the incident radiation.

However, when the magnetic field is finite, the oscillating electron also experiences the Lorentz force of $-ev^{\wedge}B$ which causes the plane of oscillation to precess about the field direction with the Larmor angular frequency given by

$$\omega_L = g_J \frac{e}{2m} B = (g_J \mu_B B)/\hbar \quad (15.2)$$

where g_J is the Landé factor for the excited 6^3P_1 level and $\mu_B = eh/2m$ is the Bohr magneton. In the absence of a polarizer, a hypothetical observer looking towards the resonance cell from the position of the detector would see the electron tracing out the paths shown in Fig.15.4. As the magnetic field strength is progressively increased, the excited electron is able to complete more and more of the rosette before its energy has been radiated away and consequently the electric field emitted suffers progressive depolarization. This precession of the classical electron is associated in the quantum-mechanical theory with the time development of the transverse magnetic moment created by the coherent excitation of the $m_J = \pm 1$ levels.

At time t , the plane of oscillation of the electron makes an angle $\{\omega_L(t-t_0)-\alpha'\}$ with the transmission axis of the polarizer, and the intensity of light recorded by the detector is given by

$$I(B, t_0) = I_0 \exp\{-\Gamma(t-t_0)\} \cos^2 \{\omega_L(t-t_0)-\alpha'\}. \quad (15.3)$$

This damped modulation of the intensity at twice the Larmor frequency has been observed in time-resolved experiments which are described in section 15.8 below. For the moment we are concerned with steady-state experiments in which the intensity of fluorescent light is measured for a sample of atoms that were excited at a constant rate, R , for all times from $t_0 = -\infty$ to the time of observation t . In this case we have

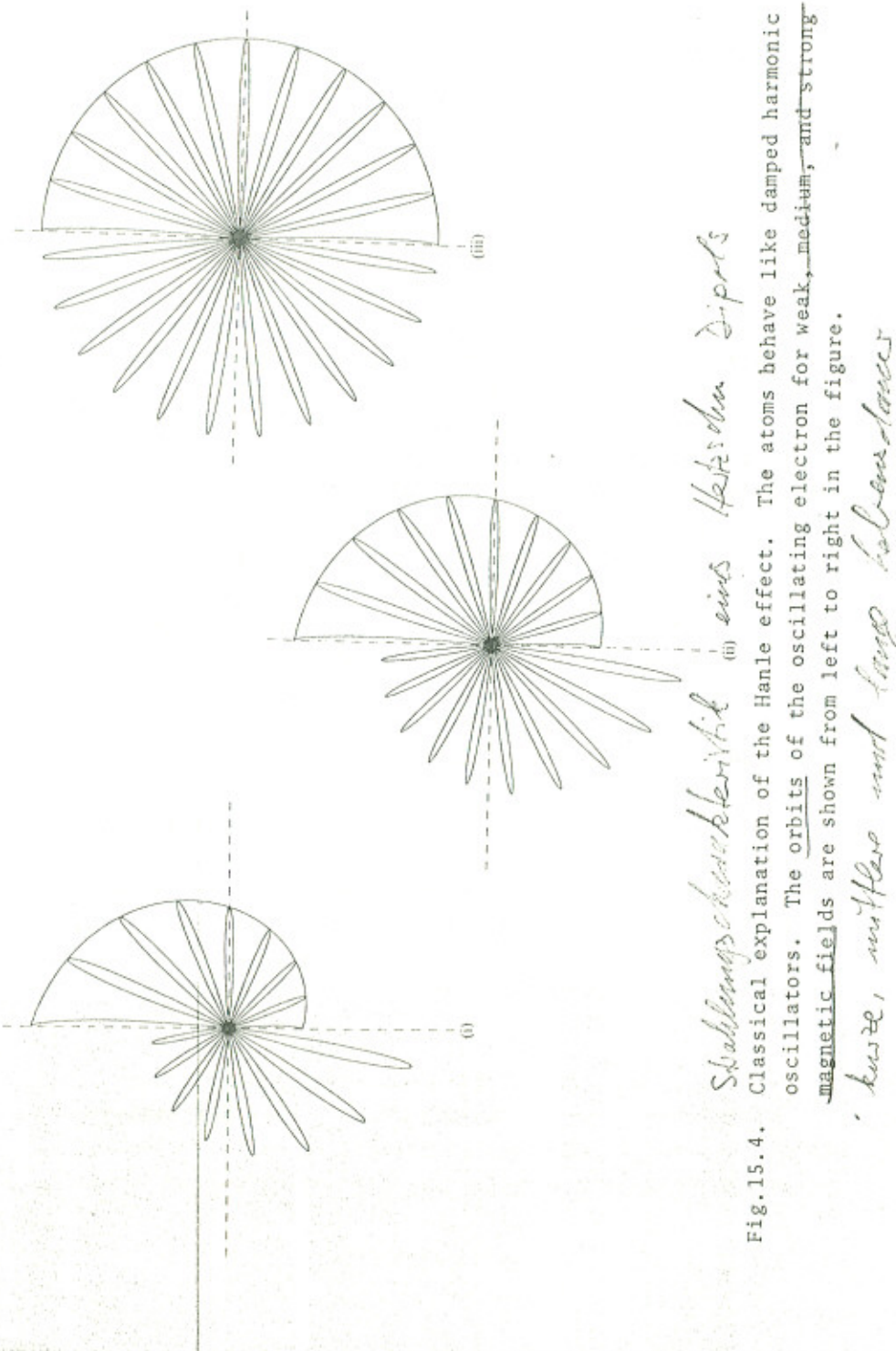


Fig. 15.4.

Classical explanation of the Hanle effect. The atoms behave like damped harmonic oscillators. The orbits of the oscillating electron for weak, medium, and strong magnetic fields are shown from left to right in the figure.

hurje, svagare och starkare bänkbevis

$$\begin{aligned}
 I(B) &= R \int_{-\infty}^t I(B, t_0) dt_0 \\
 &= \frac{I_0 R}{2} \int_{-\infty}^t \exp\{-\Gamma(t-t_0)\} [1 + \cos 2(\omega_L(t-t_0) - \alpha')] dt_0 \\
 &= \frac{I_0 R}{2} \left\{ \frac{1}{\Gamma} + \frac{\Gamma \cos 2\alpha'}{\Gamma^2 + 4\omega_L^2} + \frac{2\omega_L \sin 2\alpha'}{\Gamma^2 + 4\omega_L^2} \right\}.
 \end{aligned} \quad (15.4)$$

Thus in this experimental geometry, the shape of the Hanle effect signal depends on the orientation of the polarizer in the detection beam. The signals have a Lorentzian shape for $\alpha'=0$ or $\pi/2$ and a dispersion shape for $\alpha'=\pi/4$ or $3\pi/4$ when plotted as a function of the magnetic field dependent variable ω_L , as shown in Fig. 15.3. It is a remarkable fact that the field-dependent terms of equation (15.4) correctly describe the shape of the Hanle signals for any atomic system, regardless of the angular momentum quantum numbers that characterize the levels. A quantum-mechanical analysis is necessary only for levels with hyperfine structure or for nearly degenerate fine-structure multiplets.

15.2.4. Hanle effect width and determination of lifetimes.

Hanle effect experiments can in fact be performed in a variety of geometrical arrangements differing from that shown in Fig. 15.1 (Problem 15.1), and in some of these the use of polarized light is unnecessary. However, in most cases it is arranged that the observed signal has the Lorentzian form. In these experiments the field-dependent term falls to half its maximum value at magnetic fields B_{\pm} given by

$$\pm 2\omega_L = 2g_J\mu_B B_{\pm}/\hbar = \Gamma,$$

as shown in Fig. 15.5. The full width of the signal, ΔB , at half the maximum intensity is therefore connected with the radiative lifetime through the relation

$$g_J\mu_B \Delta B/\hbar = \Gamma = 1/\tau. \quad (15.5)$$

Thus the lifetime of the excited level may be determined

directly from the width of the measured magnetic depolarization curve provided, of course, that the Landé factor g_J of the level is known, (Problem 15.2). This width is usually obtained by a detailed fit of the theoretical lineshape to the observed signal rather than by a single measurement of ΔB at the half-intensity level.

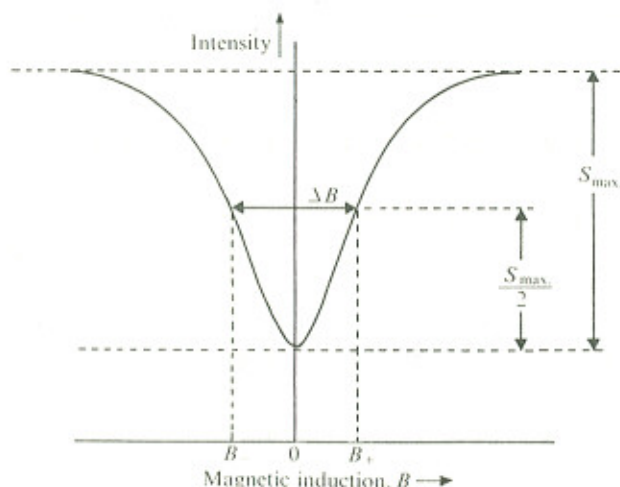


Fig. 15.5. Schematic Hanle signal with the definition of ΔB , the full width at half maximum intensity.

It is important to note that although optical radiation is being used in these experiments both for excitation and detection, the width of the depolarization signal is determined by the natural linewidth of the excited level rather than by the Doppler width of the optical line. The detection system is in fact equally sensitive to all frequencies within the line profile and the shape of the optical line is not resolved. The depolarization signal appears effectively at zero (d.c.) frequency and hence we may say that Doppler broadening is theoretically impossible.

Over the last fifteen years this simple and powerful technique has been used to obtain accurate measurements of

the radiative lifetimes of a large number of excited levels, some of which are given in Tables 15.1 and 15.2. Representative experiments in this field are described in the papers referred to in these tables. In a number of cases the recent measurements differ significantly from the results obtained by the early workers in this field and tabulated in Mitchell and Zemansky (1966). These discrepancies are generally due to the effects of radiation trapping and collisional broadening which were not thoroughly understood until about 1965. Since these effects also occur in experiments involving optical double resonance, we defer a discussion of them until Chapter 16. We now consider how the range of applicability of Hanle effect experiments has been extended by the use of electron bombardment and excitation from metastable levels.

15.3. Excitation by electron impact

It is difficult to apply the Hanle effect to levels above the resonance level using optical excitation from the ground state because of the low oscillator strength and short wavelength of many of the absorption lines.[†] Thus in an effort to extend the number of accessible levels several investigators have used electron impact excitation. It is well known that when atoms are excited by a collimated beam of electrons whose energy is at or just above the excitation threshold, the light emitted is strongly polarized. In order to create the atomic polarization necessary for Hanle effect signals using electron bombardment excitation, it is necessary that the electron velocity vector should be perpendicular to the applied magnetic field B .

In these experiments the experimental chamber usually consists of a small triode valve structure in a glass envelope sealed on to a vacuum and gas handling system, as

[†]The second members of the principal series in the alkalis Na, K, Rb, and Cs form an exception to this rule.

TABLE 15.1.

Lifetimes of the $n^2P_{3/2}$ level of alkali atoms and their isoelectronic ions obtained by resonance fluorescence experiments					
Atom or ion	Resonance line wavelength		Lifetime (ns)	Absorption f-value of D ₂ line	Reference
	D ₁ (Å)	D ₂ (Å)			
Li(n=2)	6708	6708	27.8 ± 0.8	0.50	
Na(n=3)	5896	5890	16.0 ± 0.5	0.650	(a)
Mg ⁺ (n=3)	2803	2796	3.67 ± 0.18	0.64	(b)
K(n=4)	7699	7665	26.0 ± 0.5	0.678	(c)
Ca ⁺ (n=4)	3968	3934	6.72 ± 0.20	0.66	(b)
Rb(n=5)	7948	7800	25.5 ± 0.5	0.715	(a)
Sr ⁺ (n=5)	4216	4078	6.53 ± 0.2	0.71	(b)
Cs(n=6)	8944	8521	32.7 ± 1.5	0.666	(a)
Ba ⁺ (n=6)	4934	4554	6.27 ± 0.25	0.74	(b)

(a) Schmieder *et al.* (1970)

(b) Gallagher (1967)

(c) Schmieder *et al.* (1968).

shown in Fig. 15.6. The electrons are produced by a heated oxide-coated cathode and are accelerated into the grid-anode space where atomic excitation takes place. The emitted light is detected in a manner similar to that described in

section 15.2, the only difference here being that a monochromator or narrow-band interference filter must be used to isolate the spectral line of interest. This technique has been used, for instance, in Hanle effect lifetime measurements in helium and neon (Faure *et al.* 1963).

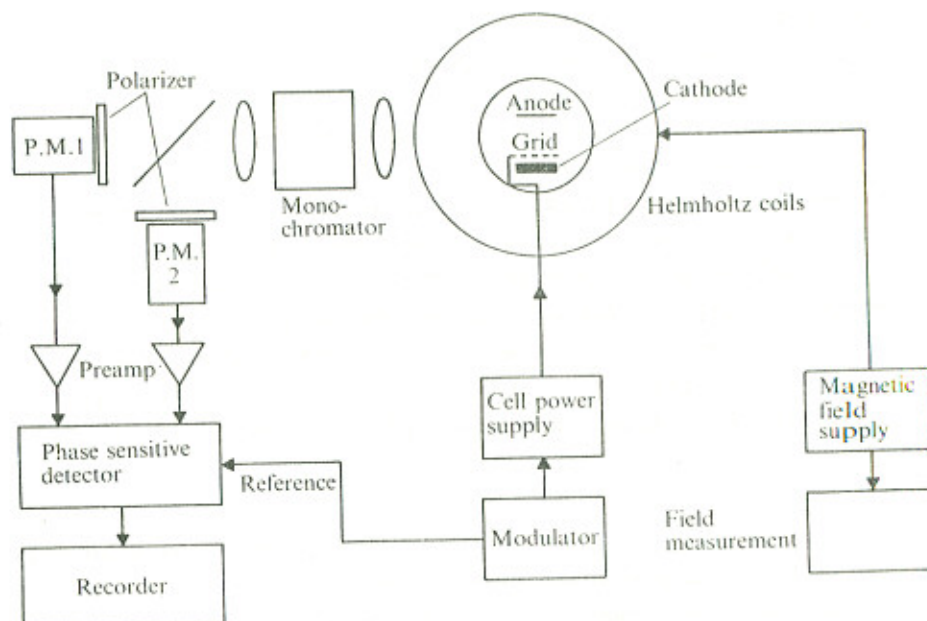


Fig. 15.6. Sample cell and electrode structure for Hanle effect and optical double-resonance experiments using electron impact excitation. (After Pebay-Peyroula (1969).)

However, electron impact excitation in hot-cathode triodes is not suitable for elements that poison the cathode or require high temperatures for vapourization. To overcome these difficulties Lombardi and Pebay-Peyroula (1965) developed a method using electron excitation in an intense r.f. discharge. The experimental chamber in this case consists of a thin cylindrical cell placed between two flat condenser plates which form the termination of a $\lambda/4$ length of r.f.

line. The principle of the technique is that at low enough pressures and with high r.f. electric field strengths between the plates of the condenser, the electrons in the discharge oscillate in a direction parallel to the applied electric field. Typical operating parameters are 0.1 Torr pressure in the cell with r.f. electric field strengths of 250 V/cm at 250 MHz. The electron mean free path is of the order of 1 mm and the mean energy is around 20 eV. This technique has been used successfully for Hanle effect experiments in Ca, Cd, and He.

Although electron excitation extends the range of levels and elements which can be studied by the Hanle effect, it suffers from the fact that an electron, moving at right-angles to the depolarizing magnetic field, experiences the Lorentz force $-ev\wedge B$. Its trajectory is no longer linear but curved and this causes the admixture of some dispersion shaped signal on the wings of an otherwise Lorentzian profile. The correction which must be made for this effect can sometimes change the measured lifetime by as much as 20 per cent and so limits the accuracy of this technique. In addition to this difficulty, the Hanle effect produced by electron excitation suffers from the problem of cascade. It often happens that the mean electron energy must be well above threshold to obtain sufficient signal. In this situation levels above that of interest are excited and the atomic polarization created in these is carried down to lower levels by radiative cascade. This situation has been treated theoretically by Nedelev (1966), and the results show that the observed signal will then be the product of the Hanle signals expected on the cascading and observed transitions, as shown in Fig. 15.8. If the lifetimes of the two levels are sufficiently different the two contributions to the experimental curve may be resolved, but this is often not the case.

Hanle effect signals have also been observed in the light emitted by d.c. rather than r.f. gas discharges. Using the apparatus shown in Fig. 15.7, Carrington and Corney (1971) were able to show conclusively that, in the neon discharge at

pressures in the range 1-10 Torr, the signals were created by optical excitation from highly populated metastable levels by absorption of the light produced within the discharge itself. Although the exciting radiation is necessarily unpolarized, the geometrical anisotropy of the excitation, which in this case is due to the use of a long, narrow discharge tube, and a suitable orientation of the magnetic field allow useful Hanle effect signals to be obtained. However, at pressures below 0.1 Torr, the mean free path of electrons within the discharge becomes sufficiently large to

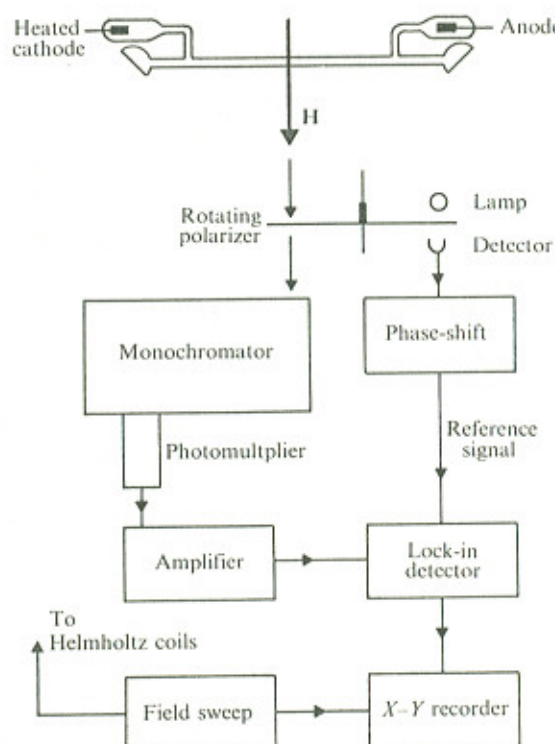


Fig. 15.7. Block diagram of the apparatus used by Carrington and Corney (1971) in studies of the Hanle effect in noble gases excited by d.c. discharges.

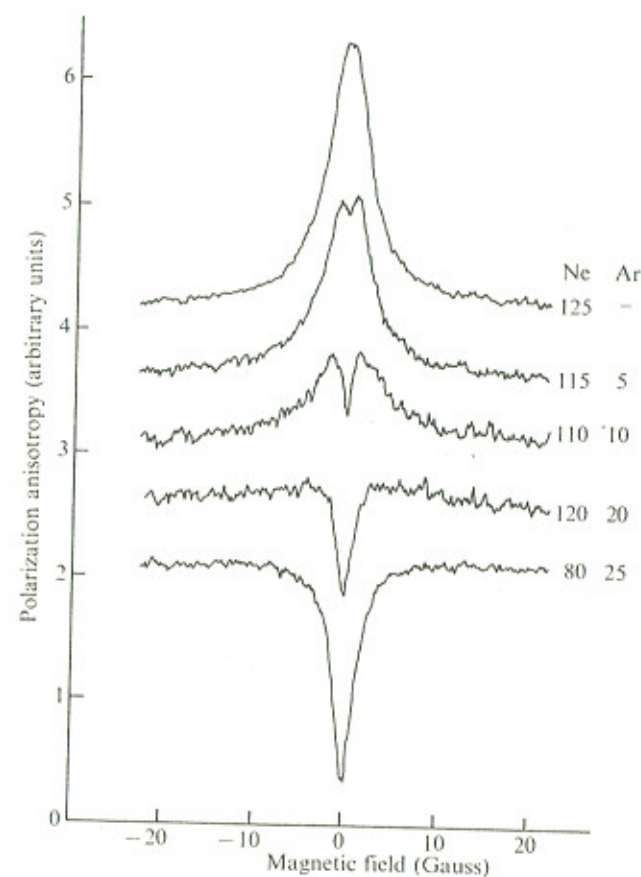


Fig. 15.8. Hanle effect on the $1s_5 - 2p_9$ transition of neon at 6402 \AA showing inversion of the signal at low pressure due to cascade of alignment from higher excited levels. Mixtures of argon and neon were used in the gas discharge and the partial pressures of the two components are shown in the diagram in mTorr. (After Carrington (1972).)

produce direct alignment, often in levels above those studied. Radiative cascade then feeds this alignment into the lower levels, just as in the case of electron excitation, and the

resulting signals have a complex shape as shown in Fig. 15.8.

Thus although the use of discharges and electron bombardment has widened the range of applicability of Hanle effect experiments, the signals are often weak and their interpretation is complicated by the large number of competing processes which occur in these systems.

15.4. Range and accuracy of lifetime measurements

The atomic lifetimes measured by the resonance fluorescence techniques range from $(2.0 \pm 0.2) \times 10^{-5} \text{ s}$ for the $4s4p\ ^3P_1$ level of zinc to $(5.69 \pm 0.23) \times 10^{-10} \text{ s}$ for the $1s2p\ ^1P_1$ level of helium, although the majority of measurements would fall in the range 10^{-6} - 10^{-9} s . The range is limited at long lifetimes by the low resonance scattering cross-section of levels with small f-values and by the effects of wall collisions in the resonance cell. Magnetic field inhomogeneities over the scattering cell are also a problem, thus for the 3P_1 level of zinc a field inhomogeneity of 1 mG over the cell would broaden the signal by approximately 10 per cent in the absence of wall collisions. Although it is possible to construct Helmholtz coils of the required homogeneity, it is difficult to eliminate the effects of stray a.c. and d.c. magnetic fields at levels below 1 mG.

At the short lifetime end of the range, the application of the Hanle effect becomes more difficult because the fields required for appreciable depolarization also produce Zeeman splittings of the states of the absorbing atom which are a substantial fraction of the Doppler width of the source. The approximation that the spectral profile of the exciting radiation is essentially flat over the absorption profile of the cell is no longer valid and it is found that the intensity of fluorescent radiation decreases on the wings of the Hanle signal. This effect has been observed in Hanle effect experiments in Hg, He, and Xe. It can be reduced to some extent by artificially broadening the lamp profile by applying a magnetic field of a few hundred gauss to the source of resonance radiation.

The relatively simple apparatus, high sensitivity, and the selective nature of the optical excitation used in many resonance fluorescence experiments combine to make this method the most accurate method for measuring atomic lifetimes. In many cases the experimental measurements may be made at densities which are so low that the effect of resonance trapping and collision broadening are completely absent. In these cases the experimental results are usually quoted with errors in the range 3-5 per cent. The method is suitable for precision lifetime measurements and may for this reason allow a set of relative oscillator strengths obtained by the absorption or emission methods to be placed on a reliable absolute basis.

The extension of the Hanle effect measurements to non-resonance levels has usually resulted in increased experimental difficulties and a consequent increase in the uncertainty of the lifetime measurements, although the results are still usually accurate to better than 10 per cent.

15.5. Theory of resonance fluorescence experiments

15.5.1. Introduction of the density matrix. We now wish to prepare the basis of the theoretical analysis which will be used to describe the resonance fluorescence experiments discussed in this and the two subsequent chapters. We are concerned with experiments in which a sample of atoms is illuminated with resonance radiation and a signal is obtained by monitoring either the intensity or the polarization of the fluorescent light. Alternatively the amount of light absorbed by the sample can be measured as in the optical pumping experiments described in Chapter 17. From the survey of quantum mechanics given in Chapter 3, we know that the most general description of the i^{th} atom in the sample involves a linear superposition of eigenfunctions with time-dependent coefficients:

$$\psi_i(t) = \sum_m a_m^{(i)}(t) |m\rangle. \quad (15.6)$$

THE HANLE EFFECT

Lifetimes of the $n\text{snp}$ 1p_1 and 3p_1 levels of Group IIB elements and the absorption f-values of the corresponding resonance lines

Atom	Multiplicity of transition	Resonance line wavelength (Å)	Lifetime (ns)	Absorption f-value	Reference
Zn($n=4$)	Singlet	2139	1.41 ± 0.04	1.46	Lurio <i>et al.</i> (1964)
	Triplet	3076	$(2.0 \pm 0.2) \times 10^4$	2.13×10^{-4}	Byron <i>et al.</i> (1964b)
Cd($n=5$)	Singlet	2288	1.66 ± 0.05	1.42	Lurio and Novick (1964)
	Triplet	3261	$(2.39 \pm 0.04) \times 10^3$	2.00×10^{-3}	Byron <i>et al.</i> (1964a)
Hg($n=6$)	Singlet	1850	1.36 ± 0.05	1.18	Lurio (1965)
	Triplet	2537	$(1.18 \pm 0.02) \times 10^2$	2.45×10^{-2}	Barrat (1959)

TABLE 15.2.

The expectation value of any physical observable, represented for instance by the operator \mathcal{M} , is then given by

$$\langle \psi_i | \mathcal{M} | \psi_i \rangle = \sum_{m,n} \rho_{mn}^{(i)} \langle n | \mathcal{M} | m \rangle \quad (15.7)$$

where

$$\rho_{mn}^{(i)} = a_m^{(i)}(t) a_n^{(i)*}(t). \quad (15.8)$$

We see that the observable properties of this atom are determined not so much by the individual coefficients $a_m^{(i)}(t)$ but by the products of the amplitudes represented by $\rho_{mn}^{(i)}$. These may conveniently be arranged in the form of a matrix. If the atomic wavefunction is changed, then the expectation value of \mathcal{M} is also changed because the matrix of the coefficients $\rho_{mn}^{(i)}$ has been altered. However, the matrix elements of the operator $\langle n | \mathcal{M} | m \rangle$ will remain the same. Alternatively if we wish to calculate the expectation value of a different operator, the matrix $(\rho_{mn}^{(i)})$ is unaltered but the operator matrix elements appearing in equation (15.7) will be changed. Thus the matrix $(\rho_{mn}^{(i)})$, called the *atomic density matrix*, would seem to be a more useful description of the system than the original atomic wavefunction.

In resonance fluorescence experiments, however, we are never able to study just a single atom, rather we are forced to investigate the properties of a sample containing N atoms. The measurable properties of this sample are then given in terms of the average values, $\langle \mathcal{M} \rangle$, of a set of physical observables taken over the ensemble of independent atoms where

$$\begin{aligned} \langle \mathcal{M} \rangle &= \frac{1}{N} \sum_{i=1}^N \langle \psi_i | \mathcal{M} | \psi_i \rangle \\ &= \frac{1}{N} \sum_{i=1}^N \sum_{m,n} \rho_{mn}^{(i)} \langle n | \mathcal{M} | m \rangle. \end{aligned} \quad (15.9)$$

For this reason it is now convenient to use the average values of the products of the probability amplitudes to define

the elements of the *density matrix* ρ of the ensemble:

$$\rho_{mn} = \langle m | \rho | n \rangle = \frac{1}{N} \sum_{i=1}^N \rho_{mn}^{(i)}. \quad (15.10)$$

From equations (15.9) and (15.10) we see that the mean value of the observable \mathcal{M} can be expressed in terms of the ensemble density matrix by

$$\langle \mathcal{M} \rangle = \sum_{n,m} \langle m | \rho | n \rangle \langle n | \mathcal{M} | m \rangle = \text{Tr}(\rho \mathcal{M}), \quad (15.11)$$

where Tr indicates that the trace of the product matrix is to be taken.

Although the density matrix is less familiar than the description in terms of atomic wavefunctions, it has the advantage that its elements have an immediate physical significance. For instance the probability of finding an atom of the vapour in the state $|m\rangle$ is given by ρ_{mm} . These diagonal elements of the density matrix also determine the magnetization of the sample when it is placed in an external magnetic field. The description of the ensemble in terms of the density matrix means that it is not necessary to know the wavefunctions of individual atoms, and indeed it may be quite impossible to write down a wavefunction for each atom owing to the effects of interatomic forces or of interactions between the atoms and the radiation fields (Problem 15.3).

15.5.2. The Liouville equation. We now derive the differential equation which controls the time development of the density matrix operator ρ . From equations (15.8) and (15.10) the rate of change of the matrix element ρ_{mn} is given by

$$\frac{\partial \rho_{mn}}{\partial t} = \frac{1}{N} \sum_{i=1}^N \{ a_m^{(i)} a_n^{(i)*} + a_m^{(i)*} a_n^{(i)} \}. \quad (15.12)$$

Since the time dependence of the probability amplitude $a_m^{(i)}(t)$ is given approximately by $\exp(-iE_m t/\hbar)$, we see that off-diagonal elements of the density matrix are periodic

functions of time with characteristic angular frequencies given by $(E_m - E_n)t/\hbar$. The detailed development of the atomic wavefunction is controlled by the Schrödinger equation

$$i\hbar \frac{\partial \psi}{\partial t} = \mathcal{H} \psi$$

once the Hamiltonian operator is specified. Substituting equation (15.6) into this equation gives

$$\dot{a}_m^{(i)} = \frac{1}{i\hbar} \sum_k \langle m | \mathcal{H} | k \rangle a_k^{(i)} \quad (15.13)$$

Using this result in equation (15.12) together with the definition of the density matrix, equation (15.10), and the Hermitian property of \mathcal{H} leads to the required differential equation:

$$\frac{\partial \rho_{mn}}{\partial t} = \frac{1}{i\hbar} \sum_k (\mathcal{H}_{mk}\rho_{kn} - \rho_{mk}\mathcal{H}_{kn}). \quad (15.14)$$

In operator form, equation (15.14) becomes

$$\frac{\partial \rho}{\partial t} = \frac{1}{i\hbar} [\mathcal{H}, \rho] \quad (15.15)$$

where the square bracket denotes the commutator product $(\mathcal{H}\rho - \rho\mathcal{H})$. This result is known as the *Liouville equation*. The theory of resonance fluorescence experiments therefore reduces to a study of the solutions of the Liouville equation for appropriate forms of the Hamiltonian operator \mathcal{H} .

15.5.3. Application of the density matrix to the theory of resonance fluorescence. Much of the theoretical development of the density matrix which follows applies equally well to all types of resonance fluorescence experiment. We shall, however, use the Hanle effect as a simple example of the general treatment. We start by assuming that the Hamiltonian \mathcal{H} , is the sum of a large time-independent operator \mathcal{H}'_0 and smaller perturbations \mathcal{H}_1 and \mathcal{H}_2 which represent the effects of optical excitation and radiative decay respectively. In this situation the Liouville equation becomes

$$\begin{aligned} \frac{\partial \rho}{\partial t} &= \frac{1}{i\hbar} [\mathcal{H}'_0, \rho] + \frac{1}{i\hbar} [\mathcal{H}_1, \rho] + \frac{1}{i\hbar} [\mathcal{H}_2, \rho] \\ &= \frac{1}{i\hbar} [\mathcal{H}'_0, \rho] + \frac{d}{dt}^{(1)} \rho + \frac{d}{dt}^{(2)} \rho. \end{aligned} \quad (15.16)$$

The time-independent Hamiltonian \mathcal{H}'_0 is itself the sum of an operator \mathcal{H}_0 , which determines the unperturbed eigenvalues and eigenfunctions of the atomic electrons, and an operator $\mathcal{H}_{\text{pert}}$, which describes the interaction of the atom with static external magnetic fields. In Chapters 16 and 17 additional terms will be introduced into equation (15.16) to account for the effects of magnetic resonance and optical pumping respectively.

In resonance fluorescence experiments we are usually interested in just two electronic levels, one of which is normally the electronic ground state. The wavefunctions required for the expansion of this restricted density matrix consist of the ground-state basis functions $|g\rangle$ and those of the excited state represented by $|e\rangle$. These wavefunctions are eigenfunctions of the angular momentum operators J_g^2 and J_e^2 with angular momentum quantum numbers given by (J_g, g) and (J_e, e) respectively.

15.5.4. The excitation process. The perturbation, \mathcal{H}_1 , represents the interaction between the atoms and the incident flux of resonance radiation. If, for the sake of simplicity the radiation field is treated classically then the perturbation has the form $\mathcal{H}_1 = -\mathbf{p} \cdot \mathbf{E}(t)$. Most of the experiments with which we shall be concerned have been performed with conventional resonance lamps. The radiation from these sources has a wide spectral bandwidth, implying very limited temporal coherence, and the spatial coherence is also very small. Thus in resonance fluorescence experiments an ensemble electric dipole moment which oscillates at the optical frequency of the incident radiation cannot be created in the sample. All off-diagonal elements of the density matrix of the form ρ_{ge} are therefore identically zero and we say that

the density matrix possesses no *optical coherence*.[†] In these experiments the density matrix therefore reduces to the sum of a ground-state part ρ_g and an excited state part ρ_e . Since at present we are chiefly interested in the time development of ρ_e , we will assume for the sake of simplicity that ρ_g has only diagonal matrix elements, i.e. $\rho_{\mu\mu'} = 0$ unless $\mu = \mu'$.

The wide spectral bandwidth of the source of resonance radiation also means that the transition of the atom from the ground to the excited level is effectively instantaneous on the time scale during which the excited atoms evolve significantly. Thus the effect of the perturbation \mathcal{H}_1 can be treated in terms of a rate process, as discussed in detail in section 9.3. When the incident radiation is in a pure state of polarization, i.e. either σ^+ , σ^- or π polarization, the atoms of the sample are excited to a pure Zeeman sub-state of the excited level. The rate at which atoms are generated in the sub-state $|m\rangle$ by optical excitation is then

$$\frac{d}{dt} \rho_{mm}^{(1)} = \sum_{\mu} P_{\mu m} \rho_{\mu\mu} \quad (15.17)$$

where $P_{\mu m}$ is the absorption transition probability given by equation (9.40). However, this result does not give a complete description of the excited state density matrix since it determines only the diagonal matrix elements of ρ_e . In Hanle effect experiments these terms are responsible for a background of resonance fluorescence which is field-independent. The magnetic depolarization signal is observed

[†]Finite values of the off-diagonal elements $\rho_{\mu m}$ would imply that the phases of the oscillating electric dipole moments induced in different atoms were coherently related to one another. Such a situation can only be achieved if the atoms are stationary and are interacting with a beam of radiation of high spatial and temporal coherence, as for instance obtained from a laser.

only when the off-diagonal elements of ρ_e are also non-zero. Since the concepts involved in this case are so important they are considered separately in the following section.

15.5.5. Radio-frequency coherence and interference of atomic states. The off-diagonal elements of the excited state atomic density matrix, $\rho_{mm'}^{(1)}$, are complex numbers whose phases ϕ_i are determined by the phase differences of the probability amplitude coefficients $a_m^{(i)}$ and $a_{m'}^{(i)}$, as shown by equation (15.8). When the average is performed over the ensemble of N atoms in equation (15.10) two different physical situations may be distinguished. In the first the ensemble of excited atoms is prepared in such a way that all values of the phase ϕ_i are equally probable. For sufficiently large N this automatically leads to the vanishing of the off-diagonal elements, $\rho_{mm'}$, of the ensemble density matrix.

In the second case the distribution of phases is not isotropic and the off-diagonal matrix elements are consequently finite, $\rho_{mm'} \neq 0$. For this to happen it is necessary that the excited atoms are prepared in such a way that the phase difference between the interfering states $|m\rangle$ and $|m'\rangle$ is the same for all atoms of the ensemble. One method of achieving this is by means of optical excitation using light which is a mixture of different polarization components. If the polarization vector of the incident radiation, $\hat{\epsilon}$, is expanded in terms of spherical unit vectors in the form

$$\hat{\epsilon} = \sum_{q=-1}^{+1} (-)^q \epsilon_q \hat{\epsilon}_{-q} \quad (15.18)$$

where $\hat{\epsilon}_0$ coincides with the axis of quantization, then we require at least two of the coefficients ϵ_q to be non-zero. In this case the rate at which the off-diagonal elements of the excited state density matrix are created is obtained by generalizing equations (9.40) and (15.17), giving:

$$\frac{d}{dt} \rho_{mm'}^{(1)} = \frac{\pi U(\omega)}{\epsilon_0 h^2} \sum_{\mu} \langle m | \hat{\epsilon} \cdot D | \mu \rangle \langle \mu | \hat{\epsilon}^* \cdot D | m' \rangle \rho_{\mu\mu} \quad (15.19)$$

To avoid confusion with the density operator, it is now more convenient to represent the energy density of the incident radiation by $U(\omega)$ and for similar reasons the electric dipole moment operator for the atom is taken as $D = -\frac{1}{2}e\vec{r}_i$. In contrast to the situation considered in section 15.5.4, the radiation now excites the atoms to a superposition of different Zeeman sub-states. In this case we may say that the polarization of the beam of radiation is coherent and that this coherence is transferred to the atoms.

Moreover, radiation which is polarization coherent possesses a finite component of angular momentum at right-angles to the magnetic field \underline{B} and this angular momentum is also transferred to the atoms at the moment of excitation. Thus finite values of the off-diagonal matrix elements $\rho_{mm'}$ also imply that there exist finite expectation values of the transverse components of the angular momentum operators (J_x), (J_y) etc. and of the transverse components of the magnetic dipole moment, $\langle M_x \rangle$ and $\langle M_y \rangle$. Again we should note that this situation only occurs when the angular momentum components of different atoms in the direction perpendicular to the axis of quantization are coherently phased rather than being oriented at random.

The time-dependence associated with the off-diagonal elements $\rho_{mm'}$ is given by $\exp\{-i(E_m - E_{m'})t/\hbar\}$ and can be regarded as a manifestation of the interference between the atomic states $|m\rangle$ and $|m'\rangle$. When these Zeeman sub-states belong to the same level of the atomic fine or hyperfine structure, the angular frequency $(E_m - E_{m'})/\hbar$ lies in the radio band and we say that the ensemble of atoms possesses radio-frequency or Hertzian coherence. Since Hanle effect experiments are performed at zero (d.c.) frequency, this Hertzian coherence manifests itself as a change in the polarization of the fluorescent light rather than as a radio-frequency beat. Radio-frequency modulation of the fluorescent light can be observed if the Hertzian coherence is generated using pulsed or modulated excitation, as described

in sections 15.8 and 15.9 below. Light beats can also be observed when the radio-frequency coherence is generated by magnetic resonance in excited levels, a topic which is considered in the following chapter.

15.5.6. The relaxation processes. The second perturbation term in equation (15.16) represents the effect of relaxation processes. At present we are concerned only with the excited-state density matrix and assume that the relaxation is due only to spontaneous emission. Since this is again an essentially random process, being triggered by the zero-point fluctuations of the vacuum radiation fields, the effect of \mathcal{K}_2 can be represented as a rate process and we have

$$\frac{d}{dt} \rho_{mm'}^{(2)} = -\Gamma \rho_{mm'}, \quad (15.20)$$

where $\Gamma = \sum_i A_{ki}$ is the spontaneous decay rate. Interatomic collisions and resonance trapping of the fluorescent radiation make additional contributions to the relaxation of the excited state but a detailed discussion of these effects is reserved until sections 16.4 and 16.5.

15.6. Theory of the Hanle effect

15.6.1. The excited-state density matrix. We now apply the general formalism developed in the previous paragraphs to the particular case of the Hanle effect. In these experiments the excited atoms are subjected to a static external magnetic field \underline{B} whose direction is chosen as the axis of quantization. In the absence of hyperfine structure the time-independent Hamiltonian for the system becomes

$$\mathcal{K}_0 = \mathcal{K}_0 + g_J \mu_B B J_z = \mathcal{K}_0 + \hbar \omega_L J_z \quad (15.21)$$

where J_z is the z-component of the dimensionless angular momentum operator introduced in section 3.6 and ω_L is the Larmor angular frequency defined by equation (15.2). The Hamiltonian operator \mathcal{K}_0 determines the unperturbed energy

levels of the atom. Using equation (15.21) in the Liouville equation (15.16), we discover that the elements of the excited-state density matrix are solutions of the equation

$$\frac{\partial \rho_{mm'}}{\partial t} = -i\omega_L(m|J_z|\rho)|m') + \frac{d}{dt}(1)\rho_{mm'} + \frac{d}{dt}(2)\rho_{mm'}, \quad (15.22)$$

Substituting the explicit expressions for the excitation and relaxation rate processes from equations (15.19) and (15.20) and using the fact that the states $|m\rangle$ and $|m'\rangle$ are eigenfunctions of the operator J_z , we have

$$\frac{\partial \rho_{mm'}}{\partial t} + i\omega_L(m-m')\rho_{mm'} + \Gamma\rho_{mm'} = \frac{\pi U(\omega)}{\epsilon_0^2 h^2} \sum_{\mu} F_{mm'} \rho_{\mu\mu} \quad (15.23)$$

where $F_{mm'} = \langle m|\underline{e}.\underline{D}|u\rangle \langle u|\underline{e}^*.\underline{D}|m'\rangle$ is often called the excitation matrix. We again note that the off-diagonal elements of the excited-state density matrix are periodic functions of time with an associated angular frequency of $\omega_L(m-m')$. It is interesting to note that the time-development of the transverse components of the excited-state magnetic dipole moment is identical to the Larmor precession of the electron oscillators introduced in the classical model of section 15.2.

In most experiments the excited atoms are created by a lamp whose intensity is independent of time and we can obtain the steady-state density matrix by setting $\dot{\rho}_{mm'}=0$ in equation (15.23), giving

$$\rho_{mm'} = \frac{\pi U(\omega)}{\epsilon_0^2 h^2} \sum_{\mu} \frac{F_{mm'} \rho_{\mu\mu}}{\Gamma + i\omega_L(m-m')} \quad (15.24)$$

We see that appreciable Hertzian coherence, implying large off-diagonal elements of ρ_e , is created only when the angular frequency $\omega_L(m-m')$ is comparable to or less than the relaxation rate Γ . Since Γ determines the width of the excited-state energy levels in angular frequency units, this coherence is destroyed when the magnetic field is large enough that different Zeeman sub-levels no longer overlap. This is the reason why Hanle effect investigations are sometimes known as zero-field level-crossing experiments.

15.6.2. The polarization of the fluorescent light. The Hanle effect signal is usually obtained by measuring the intensity of the fluorescent light with polarization vector \hat{e}' emitted in some well-defined direction \hat{l} . From equations (2.70) and (5.8) it can be shown (Problem 15.4) that the intensity of light with this polarization emitted when an excited atom in the sub-state $|m\rangle$ decays to the ground-state sub-level $|u'\rangle$ is

$$\frac{dI}{d\Omega} = \frac{\omega^3}{8\pi\epsilon_0^2 hc^3} |\langle m|\hat{e}'.\underline{D}|u'\rangle|^2 \quad (15.25)$$

when measured in terms of photons/s-steradian. To include the case of excited atoms described by an arbitrary density matrix, we generalize equation (15.25) by forming the fluorescent light monitoring operator L_F defined by

$$L_F = \frac{\omega^3}{8\pi\epsilon_0^2 hc^3} \sum_{\mu'} \langle \hat{e}'.\underline{D}|u'\rangle \langle u'|\hat{e}'^*.\underline{D}| \quad (15.26)$$

Thus the observed intensity of fluorescent light can be obtained using equations (15.11), (15.24), and (15.25) in the form

$$\begin{aligned} \frac{dI}{d\Omega} &= \text{Tr}(\rho L_F) \\ &= \frac{U(\omega)}{8\pi\epsilon_0^2} \left(\frac{\omega}{hc} \right)^3 \sum_{mm'} \frac{F_{mm'} G_{m'm}}{\Gamma + i(m-m')\omega_L} \rho_{\mu\mu'} \end{aligned} \quad (15.27)$$

where $G_{m'm} = \langle m'| \hat{e}'.\underline{D}|u'\rangle \langle u'| \hat{e}'^*.\underline{D}|m\rangle$ is called the emission matrix.

We see that field-dependent terms appear in the denominator of equation (15.27) when $m \neq m'$, i.e. the Hanle effect signal is a direct result of the Hertzian coherence created in the excited state by excitation with coherently polarized light. We can describe the phenomenon as the result of a quantum-mechanical interference between the scattering amplitudes for the two possible routes from the initial ground level sub-state $|u\rangle$ to the final sub-state

$|\mu\rangle$, as indicated diagrammatically in Fig. 15.9. This quantum-mechanical interference manifests itself as a change in the polarization and spatial distribution of the scattered resonance radiation as the separation of the Zeeman sub-states of the excited level is varied. The interference effect disappears when these levels are separated by more than their natural width Γ .

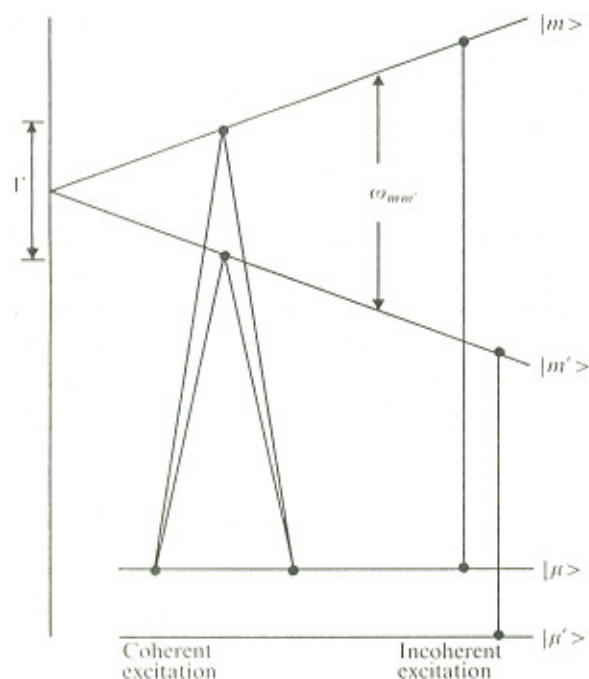


Fig. 15.9. Energy level diagram illustrating the quantum theory of the Hanle effect. The excited states $|m\rangle$ and $|m'\rangle$ are degenerate at zero magnetic field. In a finite magnetic field, the excitation of $|m\rangle$ and $|m'\rangle$ from a single ground level sub-state $|\mu\rangle$ by coherently polarized light results in interference effects in the coherently scattered radiation provided that $\omega_{mm'} = (m - m')\omega_L \leq \Gamma$ where Γ is the natural radiative width of the levels.

It should be clear from this discussion that similar effects are to be expected when the Zeeman levels of an atom with hyperfine structure intersect at large magnetic fields. These high-field level-crossing signals are discussed in detail in Chapter 18. Similar changes in the angular distribution of electromagnetic radiation are well known in nuclear physics and the perturbation of the angular correlation of cascading γ -rays produced by a large external field is widely used in the spectroscopy of excited nuclei.

15.6.3. Effect of hyperfine structure on the Hanle signal.

For an element having an odd isotope with nuclear spin I , equation (15.27) shows that the principal effect of hyperfine structure in the Hanle effect experiments will be to replace the Landé factor g_J used in the calculation of the Larmor frequency, equation (15.2), by the hyperfine g -factor g_F , where, to a good approximation

$$g_F \approx g_J \left\{ \frac{F(F+1) + J(J+1) - I(I+1)}{2F(F+1)} \right\} \quad (15.28)$$

and F is the total angular momentum quantum number of a given hyperfine component of the excited energy level. Thus, except for the case when $J=I$, the different hyperfine levels have different values of g_F and so produce Hanle effect signals with different widths. Since it is not usually possible to excite to just a single hyperfine level, the observed signal will depend on the detailed form of the emission and absorption profiles of the lamp and resonance cell respectively. It is therefore difficult to use the odd-isotope Hanle signals for accurate lifetime measurements, and experiments on pure samples of the even isotopes are to be preferred.

These are not possible in the case of sodium and potassium and here an even more complex situation arises, for these elements have an excited state hyperfine structure in zero field which is only slightly larger than the radiation width of the levels. The magnetic fields required for

the Hanle effect are sufficiently large to cause appreciable decoupling of the electronic and nuclear spin angular momentum vectors, \underline{J} and \underline{I} . In this situation the excitation of different hyperfine levels can no longer be treated as independent processes and the coherence created is responsible for level-crossing signals at finite fields. These level-crossing signals overlap the zero-field Hanle signals and therefore a detailed comparison of the experimental and theoretical signals over a wide range of magnetic fields is required to determine the lifetimes and hyperfine structure constants of the levels. This topic will be discussed again in Chapter 18.

15.7. Theory of resonance fluorescence in the $J_e=1 \rightarrow J_g=0$ case

15.7.1. Details of the experimental geometry. The excitation and emission matrices appearing in equation (15.27) are determined solely by the geometry of the apparatus and the orientation of the polarizers used. They are therefore a common feature of many different types of resonance fluorescence experiment and we demonstrate their manipulation in some detail. We consider a sample of atoms excited by a beam of resonance radiation whose direction of propagation is defined by the angles (θ, ϕ) in a spherical coordinate system. We assume that the light is linearly polarized with its electric vector making an angle α with the unit vector $\hat{\mathbf{e}}$ as shown in Fig. 15.10.

In cartesian coordinates it may be shown (Problem 15.5) that the polarization vector of the incident radiation is given by

$$\hat{\mathbf{e}} = \hat{i}(\cos\theta\cos\phi\cos\alpha - \sin\phi\sin\alpha) + \hat{j}(\cos\theta\sin\phi\cos\alpha + \cos\phi\sin\alpha) - \hat{k}\sin\theta\cos\alpha. \quad (15.29)$$

For the evaluation of the atomic matrix elements, however, it is more convenient to expand $\hat{\mathbf{e}}$ in terms of the spherical unit vectors $\hat{\mathbf{e}}_{\pm 1} = \pm \frac{1}{\sqrt{2}}(\hat{i} \pm i\hat{j})$; $\hat{\mathbf{e}}_0 = \hat{k}$ in the form given by

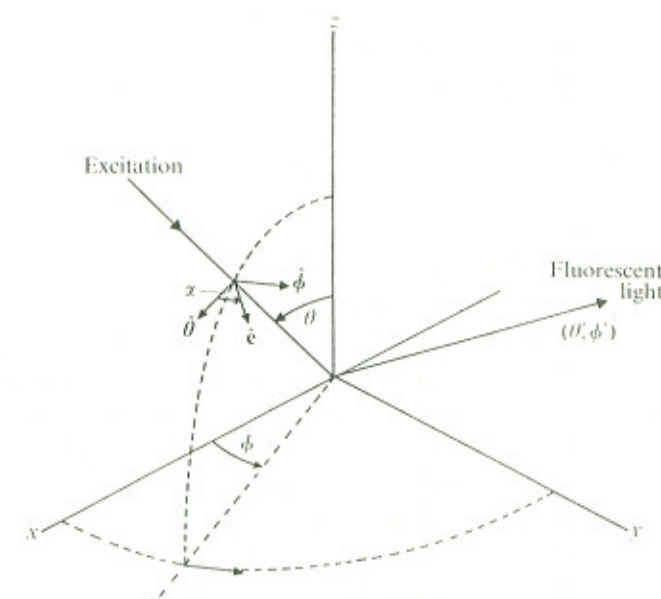


Fig. 15.10. Geometry for theoretical description of resonance fluorescence experiments.

equation (15.19). In this system we have

$$\begin{aligned} \hat{\mathbf{e}}_{\pm 1} &= \mp \frac{1}{\sqrt{2}} (\hat{\mathbf{e}}_x \pm i\hat{\mathbf{e}}_y) = \mp \frac{1}{\sqrt{2}} (\cos\theta\cos\alpha \pm i\sin\alpha)e^{\pm i\phi} \\ \hat{\mathbf{e}}_0 &= \hat{\mathbf{e}}_z = -\sin\theta\cos\alpha \end{aligned} \quad (15.30)$$

The electric dipole moment operator, \underline{D} , may be expanded in the same manner and it can then be shown that

$$\underline{e} \cdot \underline{D} = -(\hat{\mathbf{e}}_{+1} D_{-1} + \hat{\mathbf{e}}_{-1} D_{+1}) + \hat{\mathbf{e}}_0 D_0. \quad (15.31)$$

We must now evaluate the matrix elements of the electric dipole operator. We choose as an example a system in which $J_g=0$ and $J_e=1$ for the numerical values of the matrix elements in this case are particularly simple. Using equation (5.17) we have

$$\langle 0 | \hat{g}_{\pm 1} D_{\mp 1} | \pm 1 \rangle = - \langle D \rangle g_{\pm 1} \quad (15.32)$$

$$\langle 0 | \hat{g}_0 D_0 | 0 \rangle = \langle D \rangle g_0$$

where $\langle D \rangle = \langle \gamma_0 \hat{D} \gamma_1 \rangle$ is the reduced matrix element of the operator \hat{D} . The excitation matrix can now be calculated with the help of equations (15.31) and (15.32), giving

$$F_{mm'} = \langle m | \hat{e} \cdot \hat{D} | \mu \rangle \langle \mu | \hat{e}^* \cdot \hat{D} | m' \rangle = \mathcal{F}[\langle D \rangle]^2$$

where

$$\mathcal{F} = \begin{array}{c|ccc} m & m' & & \\ \hline 1 & 1 & 0 & -1 \\ 0 & -g_{+1}g_{-1} & -g_0g_{-1} & -g_{-1}^2 \\ -1 & g_{+1}g_0 & g_0^2 & g_{-1}g_0 \end{array} \quad (15.33)$$

The de-excitation matrix for light emitted in the direction (θ', ϕ') and linearly polarized parallel to the electric vector \hat{e}' is defined by

$$G_{m'm} = \langle m' | \hat{e}' \cdot \hat{D} | \mu' \rangle \langle \mu' | \hat{e}'^* \cdot \hat{D} | m \rangle \quad (15.34)$$

where \hat{e}' makes an angle α' with the direction of the unit vector $\hat{\theta}'$. In this geometry $G_{m'm}$ is identical to F_{mm} , except that all quantities in equation (15.33) are now distinguished by a prime. The matrices for the case of unpolarized light may be obtained by summing those for light polarized in directions α and $\alpha+\pi/2$ respectively.

15.7.2. Application to Hanle effect experiments. We now use the excitation and emission matrices derived above to obtain expressions for the Hanle effect signals in the $J_g=0 \leftrightarrow J_e=1$ system. These would apply, for instance, to experiments on the even isotopes of Zn, Cd, Hg, and several other elements. With the rather general geometrical arrangement of Fig. 15.10 it is convenient to separate the signal,

$dI/d\Omega$, into contributions made by terms in equation (15.27) for which $\Delta m = |m-m'|$ is constant. Using the explicit expressions for $F_{mm'}$ and $G_{m'm}$ given by equation (15.33), we then have

$$\frac{dI}{d\Omega} = \frac{dI}{d\Omega} (\Delta m=0) + \frac{dI}{d\Omega} (\Delta m=1) + \frac{dI}{d\Omega} (\Delta m=2)$$

where

$$\frac{dI}{d\Omega} (\Delta m=0) = \frac{C}{2\Gamma} (1-g_0^2 - g_0'^2 + 3g_0^2 g_0'^2) \quad (15.35)$$

$$\begin{aligned} \frac{dI}{d\Omega} (\Delta m=1) = & - \frac{2Cg_0g_0'}{\Gamma^2 + \omega_L^2} \{ \Gamma(g_{+1}g_{-1}' + g_{-1}g_{+1}') + \\ & + i\omega_L(g_{+1}g_{-1}' - g_{-1}g_{+1}') \} \end{aligned} \quad (15.36)$$

$$\begin{aligned} \frac{dI}{d\Omega} (\Delta m=2) = & \frac{C}{\Gamma^2 + 4\omega_L^2} \{ \Gamma(g_{+1}^2 g_{-1}^{'2} + g_{-1}^2 g_{+1}^{'2}) + \\ & + 2i\omega_L(g_{+1}^2 g_{-1}^{'2} - g_{-1}^2 g_{+1}^{'2}) \} \end{aligned} \quad (15.37)$$

and

$$C = \frac{U(\omega)}{8\pi\varepsilon_0^2} \left(\frac{\omega}{\hbar c} \right)^3 \langle D \rangle^4 \rho_{00}.$$

In this example ρ_{00} is the density of atoms in the ground state. This separation into three terms also has a physical significance for the density matrix of the ensemble of excited atoms can be rearranged into components which transform under rotations as tensors of rank 0, 1, and 2 respectively. These components are known as the population, orientation, and alignment of the system. In fact the different expressions given by equations (15.35)-(15.37) describe almost exactly the signals arising from the population $dI/d\Omega (\Delta m=0)$, orientation $dI/d\Omega (\Delta m=1)$, and alignment $dI/d\Omega (\Delta m=2)$ of the sample of excited atoms. We shall return to this topic when we consider the effects of relaxation by collisions and the trapping of resonance radiation in section 16.4.

For the particular geometry shown in Fig. 15.1 we have

$(\theta=\pi/2, \phi=0, \alpha=\pi/2)$ and $(\theta'=0, \phi'=\pi/2)$. By substituting these values into equation (15.30) to obtain explicit values for ϵ_q and $\epsilon_{q'}$, it can be shown (Problem 15.6) that equations (15.35)-(15.37) reduce to

$$\frac{dI}{d\Omega} (\Delta m=0) = \frac{C}{2\Gamma}$$

$$\frac{dI}{d\Omega} (\Delta m=1) = 0$$

$$\frac{dI}{d\Omega} (\Delta m=2) = \frac{C}{\Gamma^2 + 4\omega_L^2} (\Gamma \cos 2\alpha' + 2\omega_L \sin 2\alpha')$$

a result which is identical to that obtained by the classical theory, equation (15.4). This detailed analysis proves the validity of the statement made in section 15.2 that the shapes of the Hanle effect signals are correctly predicted by the classical theory. However, in systems other than the $J_g=0 \leftrightarrow J_e=1$ we can see by referring to equation (5.18) that the field-dependent term is generally a smaller fraction of the constant background signal arising from the terms with $\Delta m=0$. This reduces the signal-to-noise level and may necessitate the use of phase-sensitive detectors or other signal averaging techniques.

15.7.3. Effect of deviations from perfect geometry. In most resonance fluorescence experiments lenses and light pipes subtending large solid angles are used in both the exciting and detection arms of the apparatus in order to increase the size of the signal. In this situation the observed signal must obviously be obtained by averaging the expressions given in equations (15.35)-(15.37) over the finite solid angle used. The main result of this in a geometry where the pure Lorentzian-shaped $\Delta m=2$ signal is expected is to cause some slight admixtures of the dispersion-shaped $\Delta m=2$ signal, and possibly contributions from the $\Delta m=1$ signals as well. This leads to a slight asymmetry and broadening of the observed signals which can usually be corrected in the

analysis of the data.

15.7.4. Estimate of the size of the signal. The size of the resonance fluorescence signal is determined by the rate Q at which photoelectrons are produced at the cathode of the photomultiplier by the scattered light. In equilibrium the rate at which photons are re-emitted is equal to the rate at which they are absorbed, which in turn is determined by the effective absorption cross-section, σ_{eff} . Thus for a resonance cell of length d and cross-sectional area A which is filled with absorbing atoms at a uniform density n , we have

$$Q = F A d n \sigma_{\text{eff}} K \quad (15.38)$$

where F is the flux of resonance radiation photons incident on the cell, and K is the combined collection and detection efficiency factor. The effective cross-section may be obtained from equation (9.51) by multiplying the total absorption cross-section by the normalization factor for the folding integral of the Gaussian emission and absorption profiles of the resonance lamp and cell, giving

$$\sigma_{\text{eff}} = 4\pi \left(\frac{\pi \ln 2}{\Delta\omega_s^2 + \Delta\omega_c^2} \right)^{1/2} r_0 c f_{ik} \quad (15.39)$$

where $\Delta\omega_s$ and $\Delta\omega_c$ are the Doppler widths of the light source and absorbing atoms respectively. The large value of the resonance scattering cross-section is one of the main reasons for the great sensitivity of resonance fluorescence experiments. The factor K in equation (15.38) is given by the quantum efficiency of the photomultiplier multiplied by the solid angle subtended by the collection optics expressed as a fraction of 4π .

For typical values of the parameters in equations (15.38) and (15.39), we find (Problem 15.7) that $Q \approx 3 \times 10^7 \text{ s}^{-1}$. This is much larger than either the dark current of the photomultiplier ($\approx 10^3 \text{ s}^{-1}$) or the shot noise due to random fluctuations in the photon counting

statistics ($\approx Q^{1/2}$). Thus in many resonance fluorescence experiments excellent signal-to-noise ratios can be obtained, and experiments at very low densities or using only milligram quantities of mass-separated stable or radioactive isotopes are possible. However, equation (15.38) does emphasize the need for intense light sources in these experiments and the importance of achieving high collection and detection efficiency for the fluorescent light.

15.8. Resonance fluorescence experiments using pulsed excitation

15.8.1. Introduction and experimental techniques. In previous sections we drew attention to the fact that, in both the classical and quantum theories, expressions derived for the intensity of resonance fluorescence from atoms subjected to an external magnetic field, equations (15.3) and (15.23) respectively, contain terms which may lead to a modulation of the intensity at the Larmor frequency or its second harmonic. This radio-frequency modulation has been observed in several different kinds of experiment, the simplest of which makes use of pulsed excitation and time-resolved detection of the fluorescent light.

The first of these experiments were performed simultaneously by Dodd *et al.* (1964) and Aleksandrov (1964). The improved apparatus used by Dodd *et al.* (1967) in a more detailed study of this phenomenon is shown in Fig. 15.11. Resonance fluorescence in cadmium vapour excited by the intercombination line $5^1S_0 - 5^3P_1$ at 3261 \AA was chosen for this investigation. The cadmium atoms in a heated resonance cell were excited to the 5^3P_1 level by a pulse of resonance radiation lasting $0.2\mu\text{s}$. This excitation pulse was obtained by passing the light from a commercial cadmium lamp through a Kerr cell shutter operated by a high voltage pulse unit. The time dependence of the resonance fluorescence emitted in a direction at right-angles to both the magnetic field and the direction of the incident light was

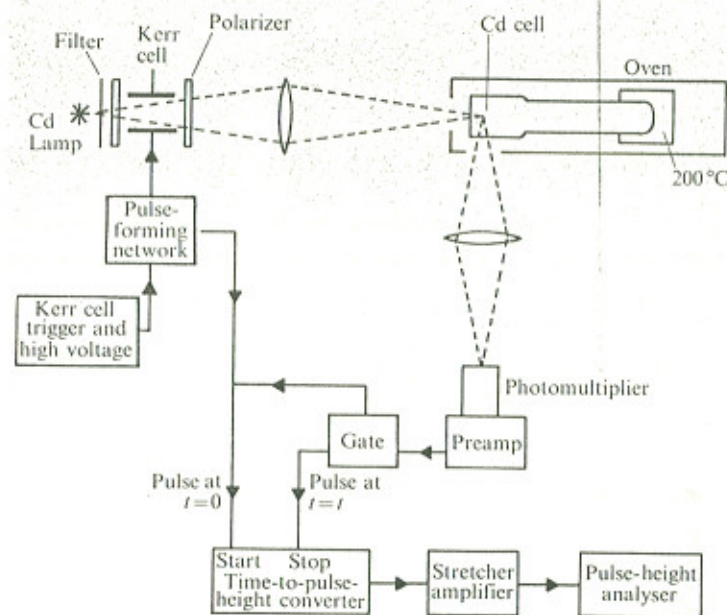


Fig. 15.11. Block diagram of the apparatus of Dodd *et al.* (1967) for cadmium resonance fluorescence experiments using pulsed excitation.

studied using the single-photon counting techniques described in section 6.3.3. The result of a seven-hour-long run obtained with the cadmium vapour at 200°C and an applied magnetic field of 345 mG is shown in Fig. 15.12(a). This displays the number of counts recorded in each channel of the analyser after a correction has been made for the background produced by photomultiplier dark current pulses and by the light reflected from the cell walls. The experimental trace can clearly be resolved into two distinct contributions consisting of a decaying but unmodulated intensity and a damped intensity modulation as shown in Figs. 15.12(b) and (c) respectively. The observed angular frequency of modulation was $(9.25 \pm 0.30) \times 10^6 \text{ s}^{-1}$, in good agreement with that predicted from the known g_J factor for the 5^3P_1 level Problem (15.9).

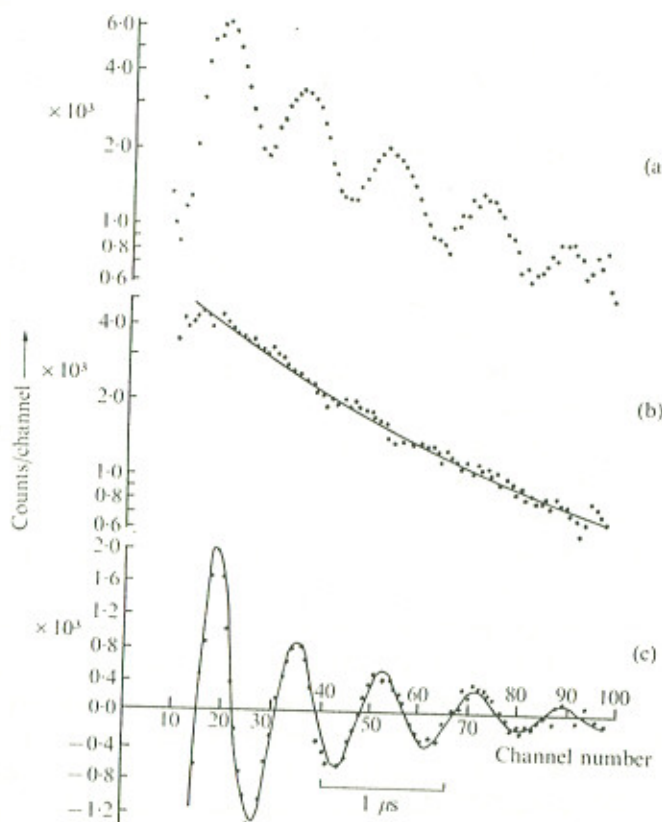


Fig. 15.12. Transient decay of cadmium atoms excited by a pulse of polarized resonance radiation. (a) The experimentally observed fluorescence as a function of time. (b) The exponential decay of unmodulated fluorescent light. (c) The modulated component of the fluorescent light. The modulation is produced by Larmor precession in the applied magnetic field of 345 mG. (After Dodd *et al.* (1967).)

15.8.2. Theoretical interpretation. For the moment we concentrate on the interpretation of the signal shown in Fig. 15.12(c). The phenomenon can be explained classically by imagining that the exciting pulse created a set of electric dipole oscillators with their axes all initially aligned parallel to the electric vector of the incident radiation (Problem 15.9). Subsequently these dipoles precess at the Larmor angular frequency about the magnetic field direction while simultaneously they suffer damping by re-radiation. The angular distribution of the electric dipole radiation pattern then produces maxima in the observed intensity every time that the axis of the dipoles is at right-angles to the direction of observation.

A general expression for the intensity of light observed in these experiments may be obtained using the density matrix formalism developed in section 15.6. We rewrite equation (15.23) allowing for the fact that the energy density of the incident radiation, $U(\omega, t)$, is now a function of time:

$$\frac{\partial \rho_{mm'}}{\partial t} + (\Gamma + ix)\rho_{mm'} = \frac{\pi U(\omega, t)}{\epsilon_0 h^2} \sum_{\mu} F_{mm'} \rho_{\mu\mu} \quad (15.40)$$

where $x = \omega_L(m-m')$. Multiplying by the integrating factor $\exp\{(\Gamma + ix)t\}$ gives

$$\frac{d}{dt} [\rho_{mm'} \exp\{(\Gamma + ix)t\}] = \frac{\pi}{\epsilon_0 h^2} \sum_{\mu} F_{mm'} \rho_{\mu\mu} U(\omega, t) \exp\{(\Gamma + ix)t\}. \quad (15.41)$$

For the sake of simplicity we now assume that the pulse of incident radiation has a rectangular shape,

$$\begin{aligned} i.e. U(\omega, t) &= U(\omega) \quad \text{for } t_0 < t < t_0 + \Delta t_0 \\ &= 0 \quad \text{for all other values of } t. \end{aligned}$$

Then integrating equation (15.41) we have for $t > t_0 + \Delta t_0$:

$$\rho_{mm'}(t) = \frac{U(\omega)\pi}{\epsilon_0 h^2} \sum_{\mu} F_{mm'} \rho_{\mu\mu} [\exp\{(\Gamma+ix)(t_0 + \Delta t_0)\} - \exp\{(\Gamma+ix)t_0\}] \times \frac{\exp\{-(\Gamma+ix)t\}}{\Gamma+ix} \quad (15.42)$$

where we have assumed that all the atoms in the sample are in the ground state before the arrival of the excitation pulse, i.e. $\rho_{mm'}(t)=0$ for $t < t_0$. The terms in equation (15.42) which involve Δt_0 are dependent on the length of the exciting pulse. The simplest situation occurs when the pulse is very much shorter than either the radiative lifetime or the period associated with the Larmor precession, i.e. $\Gamma\Delta t_0 < \omega_L \Delta t_0 \ll 1$. In this limit we find that equation (15.42) reduces to

$$\rho_{mm'}(t) = \frac{U(\omega)\pi}{\epsilon_0 h^2} \sum_{\mu} F_{mm'} \rho_{\mu\mu} \exp\{-(\Gamma+ix)(t-t_0)\}. \quad (15.43)$$

Finally, applying the monitoring operator L_F , we obtain a general expression for the intensity of fluorescent light in experiments using pulsed excitation:

$$\frac{dI}{dt} = \frac{U(\omega)}{8\pi\epsilon_0^2} \left(\frac{\omega}{hc} \right)^3 \sum_{mm'} \sum_{\mu\mu'} F_{mm'} G_{m'm} \rho_{\mu\mu} \exp\{-(\Gamma+i\omega_L(m-m'))(t-t_0)\}. \quad (15.44)$$

This calculation makes it clear that light beats are associated with the time evolution of the off-diagonal elements of the excited-state density matrix. Consequently they can only be observed in pulsed experiments if the light which excites the atoms of the sample is also polarization coherent. Only then is the necessary Hertzian coherence created in the excited-state density matrix. The theory predicts that modulation at the angular frequencies ω_L and $2\omega_L$ will be detectable depending on the geometry and polarization used in the experiment.

15.8.3. Application to the $J_e=1$ case. In the notation of section 15.7.1 the geometrical arrangement used by Dodd *et al.*(1967), and shown in Fig.15.11, is described by the

directions ($\theta=\pi/2$, $\phi=0$, $\alpha=\pi/2$) and ($\theta'=\pi/2$, $\phi'=\pi/2$). The excitation and emission matrices for this geometry may be evaluated using equations (15.30) and (15.33) and it can then be shown that the signal predicted by equation (15.44) is given by

$$\frac{dI}{dt} = \frac{C}{2} [1 - \cos\{2\omega_L(t-t_0)\}] \exp\{-\Gamma(t-t_0)\} \quad (15.45)$$

where the signals obtained with the analyser at angles of α' and $\alpha'+\pi/2$ have been summed corresponding to the detection of unpolarized light.

The theory therefore predicts an intensity modulation of 100 per cent in this geometry when the excitation pulse is sufficiently short. For pulses which do not satisfy the condition $\omega_L \Delta t_0 \ll 1$ it is found that the depth of modulation is reduced and that there is a phase shift in the modulation term. The reason for this can be easily visualized on the classical model, for the Larmor precession during a long excitation pulse causes the dipoles to be distributed through an angle $\omega_L \Delta t_0$ in the plane perpendicular to B , rather like a fan. In the limit that $\omega_L \Delta t_0 \gg 1$, the dipoles are isotropically distributed in this plane and no modulation is observed.

In the experiments of Dodd *et al.*(1967) the short pulse criteria is reasonably well satisfied since $\omega_L \Delta t_0 \approx 0.14$ and the reduced depth of modulation apparent in Fig.15.12(a) is due to depolarization by collisions with foreign gases contaminating the resonance cell. Fluorescence from the $F=1/2$ levels of the odd isotopes ^{111}Cd and ^{113}Cd (both $I=1/2$), which have a total abundance of 25 per cent in the natural cadmium used in the resonance cell, also contribute to this background since in this geometry interference effects from levels separated by $\Delta m=1$ are not observable. The signal from the $F=3/2$ level of the odd isotopes is modulated, however, at a frequency which is $2/3$ of that of the even isotope signal, as evaluation of equation (15.28) will show. This small additional component of the fluorescent light can be

clearly identified by detailed analysis of the experimental data.

One of the principal difficulties in these time-resolved experiments is the low intensity of the conventional sources of pulsed resonance radiation, as the seven-hour running time of Dodd *et al.* (1967) emphasizes. Excitation by means of pulsed tunable dye lasers seems likely to overcome this difficulty and we now briefly refer to some recent experiments using this technique.

15.8.4. Pulsed laser excitation. Quantum beats produced by dye laser excitation have been observed by Gornik *et al.* (1972) on the $6\ s^2\ ^1S_0$ - $6s6p\ ^3P_1$ intercombination line of ytterbium at 5556\AA . In this experiment the conventional resonance cell was replaced by an atomic beam of ytterbium and the atoms were excited by radiation from a nitrogen laser-pumped dye laser using a solution of sodium fluorescein and esculin in methyl alcohol. The dye laser radiation was linearly polarized in a direction at right-angles to the magnetic field applied to the atoms in the scattering chamber and the laser output was tuned on to the resonance line by a combination of three tilted solid quartz étalons and an interference filter. At a pulse repetition rate of 30 Hz a peak output power of several hundred watts was obtained with a spectral bandwidth of $< 50 \times 10^{-3}\text{ cm}^{-1}$. The laser pulse length of 7 ns is approximately a hundred times shorter than the radiative lifetime of the 3P_1 level, thus the analysis of section 15.8.2 may be applied without any modification.

The fluorescent light from the atomic beam was monitored by a photomultiplier and recorded in a Tektronix transient analyser. Quantum beat signals having excellent signal-to-noise ratios and displaying 100 per cent depth of modulation could be obtained with a single pulse of excitation. From a measurement of the modulation frequency (2.99 MHz) and a knowledge of the applied magnetic field (0.714 G), the Landé g-factor for the 3P_1 level may be obtained to an accuracy of about one per cent. Moreover the exponential envelope of the signal yields a radiative lifetime of

$\tau(6\ ^3P_1) = 860 \pm 43$ ns, in good agreement with previous determinations.

The g-factors and lifetimes of the lowest-lying 1P_1 states in barium and calcium have also been measured using the quantum beat technique by Schenck *et al.* (1973). However, a much larger number of lifetime measurements have been made in zero magnetic field by simply observing the exponential decay of the fluorescent light following dye laser excitation on a fast oscilloscope. A representative sample of the available results is given in Table 15.3. As the table indicates, this new technique is applicable to measurements over a wide range of lifetimes. Perhaps equally interesting is the new information on collisional quenching cross-sections which may also be obtained by this selective optical excitation method.

TABLE 15.3.

Radiative lifetimes of atomic and molecular levels obtained using pulsed dye laser excitation

Atom or molecule	Level	Lifetime	Reference
Na	$3p\ ^2P_{1/2}$	16.4 ± 0.6 ns	Erdmann <i>et al.</i> (1972)
Ca	$4s5s\ ^3S_1$	10.7 ± 1.0 ns	Gornik <i>et al.</i> (1973)
Mg	$3s3p\ ^3P_1$	2.2 ± 0.2 ms	Wright <i>et al.</i> (1974)
I ₂	$B\ ^3\Pi_{0u}^+$ ($v'=0 - v'=25$)	$1.6 - 2.1$ μ s	Sakurai <i>et al.</i> (1971)
Br ₂	$B\ ^3\Pi_{0u}^+$ ($v'=1 - v'=31$)	$0.14 - 1.3$ μ s	Capelle <i>et al.</i> (1971)
NO ₂	Unknown	$41 - 43$ μ s	Sakurai and Capelle (1970).

15.9. Resonance fluorescence experiments using modulated excitation

15.9.1. Introduction and experimental technique. The classical theory of resonance fluorescence, in which the atoms are treated as dipole oscillators precessing at the Larmor frequency, leads one to predict that interesting effects will also occur if the atoms are excited by light whose intensity is periodically modulated. As the external magnetic field is varied in these experiments a point is reached at which the Larmor frequency, ω_L , equals the angular frequency of the modulation, f . Additional atoms will then be excited in phase with the Larmor precession of those already in the upper state and a significant transverse magnetic moment is built up in the ensemble of excited atoms. We would therefore expect a resonant increase in the amplitude of modulation of the fluorescent light when the condition $\omega_L = f$ is satisfied.

The first resonance fluorescence experiments using intensity-modulated excitation were performed by Aleksandrov (1963) and independently by Corney and Series (1964 a,b). The apparatus used by Corney (1968) in a more detailed investigation of the phenomenon is shown in Fig. 15.13. The 5^3P_1 level of cadmium was again chosen for study. The light source was an electrodeless capillary discharge tube made from fused silica and was excited by applying a radio-frequency voltage at 231 kHz to external electrodes of aluminium sheet. It was found that the radiation from the lamp was intensity modulated at 462 kHz owing to a 100 per cent modulation of the mean energy of the electrons in the discharge which occurs at twice the frequency of the applied voltage (Harries and von Engel 1954). However, the depth of modulation of the 3261 Å radiation emitted by the lamp was only of the order of 1 per cent, indicating that direct electron impact excitation accounts for only a small fraction of the total population of the 5^3P_1 level. The light from the discharge was focussed on to a cylindrical resonance cell in an oven heated by hot air to 200°C. The

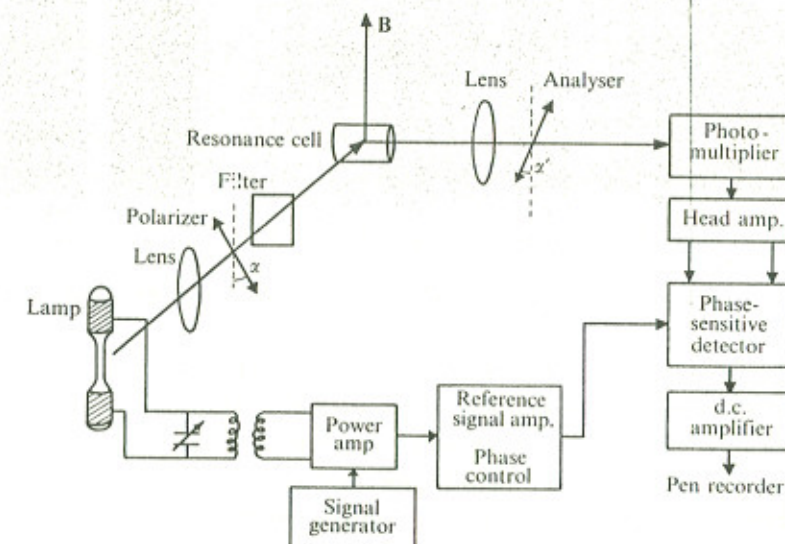


Fig. 15.13. Schematic diagram of the apparatus used in resonance fluorescence experiments on cadmium vapour excited by intensity-modulated light.

magnetic field was produced by a Helmholtz coil pair having a mean diameter of 24.9 cm and was uniform to 2 per cent over the volume of the cell. Stray d.c. magnetic fields were reduced to less than 0.5 mG using three mutually orthogonal Helmholtz coil pairs and care was taken to eliminate stray a.c. fields by careful location of electronic equipment.

The intensity of the fluorescent light was monitored by a photomultiplier and the time-dependent signal was isolated by an amplifier tuned to 462 kHz. The radio-frequency modulation of the fluorescent light was readily confirmed by this method, but the small percentage modulation of the incident light made phase-sensitive detection essential for detailed studies. This technique had the advantage that the amplitudes of the in-phase and quadrature components

of the fluorescent radiation,

$$I(t) = A \cos ft + B \sin ft,$$

could be studied separately.

15.9.2. Experimental results. In the experimental geometry shown in Fig. 15.13 atoms were excited to a coherent superposition of the $m_J = \pm 1$ states when the incident light was polarized at right-angles to the field direction. An experimental recording of the amplitude of the in-phase component of modulation of the fluorescent light is shown in Fig. 15.14 (a) as a function of the applied magnetic field. The trace consists of two Lorentzian shaped resonances, overlapping slightly in the region of zero magnetic field, and centred at fields of ± 0.110 G. At these values of the magnetic field the $m_J = \pm 1$ states of the excited atom are separated by a frequency interval $2\omega_L/2\pi = 462$ kHz, as expected. The resonances can thus be regarded as the effect of interference between the σ^+ and σ^- polarized Zeeman components of the fluorescent light. The theory developed in the next section shows that the amplitude of the in-phase component is given by

$$A = \left\{ \frac{2\Gamma}{\Gamma^2 + f^2} - \frac{\Gamma}{\Gamma^2 + (2\omega_L + f)^2} - \frac{\Gamma}{\Gamma^2 + (2\omega_L - f)^2} \right\} I_0 \Gamma. \quad (15.46)$$

This expression was evaluated using the experimental lifetime for the 5^3P_1 level of $\tau = 2.25 \times 10^{-6}$ s obtained by Barrat and Butaux (1961), and is plotted in Fig. 15.14(b). The agreement between the experimental and theoretical curves is very satisfactory.

15.9.3. Theory of resonance fluorescence excited by modulated light. Theoretical expressions for the intensity of light observed in resonance fluorescence experiments using modulated excitation can be obtained by a simple extension of equation (15.41). We now assume that the energy density of the incident radiation, $U(\omega, t)$, is amplitude modulated at

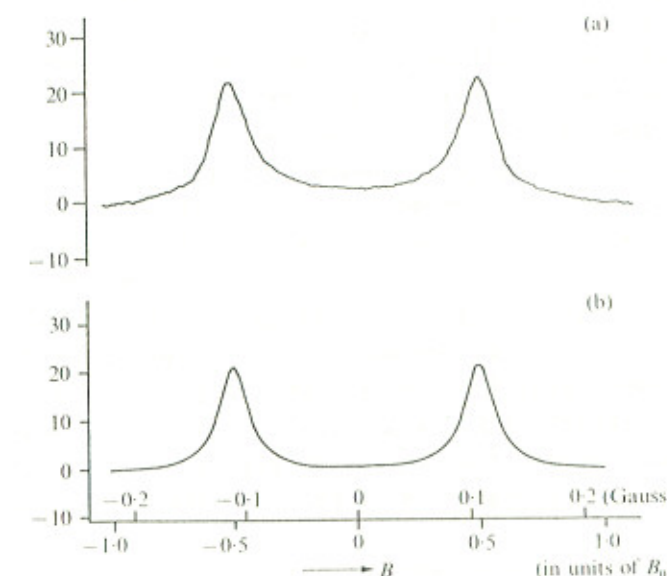


Fig. 15.14. Study of the fluorescent radiation from a sample of cadmium atoms excited by light which is intensity modulated at the frequency $f/2\pi = 462$ kHz. (a) Experimental recording of the in-phase component of the modulated fluorescence as a function of applied field, B . (b) Plot of the theoretical expression, equation (15.46). Resonances occur when $B = \pm B_0/2$ where $B_0 = hf/gJ\mu_B$.

the angular frequency f . Thus $U(\omega, t)$ is given by

$$U(\omega, t) = U(\omega) (1 + a \cos ft) \quad (15.47)$$

where a is the depth of modulation. Substituting into equation (15.41), we have

$$\frac{d}{dt} [\rho_{mm}, \exp\{(\Gamma+ix)t\}] = \frac{\pi U(\omega)}{\epsilon_0 h^2} \sum_\mu F_{mm,\mu} \rho_{\mu\mu} (1 + a \cos ft) \exp\{(\Gamma+ix)t\}. \quad (15.48)$$

Integrating over t from $t = -\infty$ to the instant of observation

t , and assuming $\rho_{mm}(-\infty)=0$, we have

$$\rho_{mm}(t) = \frac{\pi U(\omega)}{8\pi\epsilon_0^2} \sum_{\mu} F_{mm} \rho_{\mu\mu} \left[\frac{1}{\Gamma+i(x+f)} + \frac{a}{2} \left\{ \frac{\exp(ift)}{\Gamma+i(x+f)} + \frac{\exp(-ift)}{\Gamma+i(x-f)} \right\} \right]. \quad (15.49)$$

Finally, introducing the monitoring operator L_F , the general expression for the intensity of fluorescent light is given by

$$\frac{dI}{d\Omega} = \frac{U(\omega)}{8\pi\epsilon_0^2} \left(\frac{\omega}{hc} \right)^3 \sum_{\substack{mm' \\ \mu\mu'}} F_{mm'} G_{m'm} \rho_{\mu\mu'} \times \times \left[\frac{1}{\Gamma+i(x)} + \frac{a}{2} \left\{ \frac{\exp(ift)}{\Gamma+i(x+f)} + \frac{\exp(-ift)}{\Gamma+i(x-f)} \right\} \right] \quad (15.50)$$

where $x=\omega_L(m-m')$.

This general expression consists of a sum of time-independent terms which describe the usual Hanle effect signals and terms modulated at the angular frequency f which are resonant when $\omega_L(m-m') = \pm f$. These terms control the amplitude of modulation of the fluorescent light and originate in the off-diagonal elements of the excited state density matrix. When the condition $f \gg \Gamma$ is satisfied, excitation by amplitude-modulated light creates substantial Hertzian coherence at fields which are well separated from the zero-field level-crossing region.

15.9.4. Application to $J_c=1$ case. The geometrical arrangement shown in Fig.15.13 is described by the angles $(\theta=\pi/2, \phi=0, \alpha)$ and $(\theta'=0, \phi'=\pi/2, \alpha')$ in the notation of section 15.7.1. Using equations (15.30) and (15.33) to evaluate the excitation and emission matrices in this geometry we obtain, after substitution in equation (15.50),

$$\begin{aligned} \frac{dI}{d\Omega} (\Delta m=0) &= C(\cos^2\alpha \cos^2\alpha' + \frac{1}{2}\sin^2\alpha \sin^2\alpha') \\ &\times \left\{ \frac{1}{\Gamma} + \frac{a}{2} \left(\frac{2\Gamma \cos ft}{\Gamma^2+f^2} + \frac{2f \sin ft}{\Gamma^2+f^2} \right) \right\}. \end{aligned} \quad (15.51a)$$

$$\begin{aligned} \frac{dI}{d\Omega} (\Delta m=1) &= C \frac{\sin 2\alpha \sin 2\alpha'}{2} \left[\frac{\omega_L}{\Gamma^2+\omega_L^2} + \right. \\ &+ \frac{a}{2} \cos ft \left\{ \frac{\omega_L - f}{\Gamma^2+(\omega_L - f)^2} + \frac{\omega_L + f}{\Gamma^2+(\omega_L + f)^2} \right\} + \\ &\left. + \frac{a}{2} \sin ft \left\{ \frac{\Gamma}{\Gamma^2+(\omega_L - f)^2} - \frac{\Gamma}{\Gamma^2+(\omega_L + f)^2} \right\} \right] \end{aligned} \quad (15.51b)$$

$$\begin{aligned} \frac{dI}{d\Omega} (\Delta m=2) &= C \frac{\sin^2 \alpha \sin^2 \alpha'}{2} \left[\frac{\Gamma}{\Gamma^2+4\omega_L^2} + \right. \\ &+ \frac{a}{2} \cos ft \left\{ \frac{\Gamma}{\Gamma^2+(2\omega_L + f)^2} + \frac{\Gamma}{\Gamma^2+(2\omega_L - f)^2} \right\} + \\ &\left. + \frac{a}{2} \sin ft \left\{ \frac{2\omega_L + f}{\Gamma^2+(2\omega_L + f)^2} - \frac{2\omega_L - f}{\Gamma^2+(2\omega_L - f)^2} \right\} \right]. \end{aligned} \quad (15.51c)$$

The time-independent terms in equations (15.51a,b,c) describe Hanle effect signals excited by the unmodulated component of the incident radiation density, equation (15.47), while the time-dependent terms in equation (15.51a) describe the phase shift and depth of modulation which is expected when a system having a damping constant Γ is periodically excited (Problem 15.10). Since this is a population effect these terms are independent of the applied magnetic field. By contrast the time-dependent terms in equations (15.51b,c) are resonant at fields given by $\omega_L = \pm f$ and $2\omega_L = \pm f$, corresponding to interferences between states with $\Delta m=1$ and $\Delta m=2$ respectively. These resonances in the amplitude of modulation have the familiar Lorentzian or dispersion lineshape, depending on the phase of the modulation detected.

The signals shown in Fig.15.14a were obtained in this geometry by detecting unpolarized fluorescent light. The required theoretical expression is obtained from equation (15.51) by summing expressions with the polarizer angles set at α' and $\alpha'+\pi/2$. The contributions from the terms with $\Delta m=1$ vanish, corresponding to the fact that the orthogonal states of polarization, σ and π , of the fluorescent

light can no longer interfere. In this case equation (15.51) reduces to

$$\begin{aligned}\frac{dI}{d\Omega} (\Delta m=0) &= \frac{C}{2}(1+\cos^2 \alpha) \left[\frac{1}{\Gamma} + \frac{a}{2} \left(\frac{2\Gamma \cos ft}{\Gamma^2 + f^2} + \frac{2f \sin ft}{\Gamma^2 + f^2} \right) \right], \\ \frac{dI}{d\Omega} (\Delta m=2) &= -\frac{C}{2} \sin^2 \alpha \left[\frac{r}{\Gamma^2 + 4\omega_L^2} + \right. \\ &\quad + \frac{a}{2} \cos ft \left\{ \frac{\Gamma}{\Gamma^2 + (2\omega_L + f)^2} + \frac{\Gamma}{\Gamma^2 + (2\omega_L - f)^2} \right\} + \\ &\quad \left. + \frac{a}{2} \sin ft \left\{ \frac{2\omega_L + f}{\Gamma^2 + (2\omega_L + f)^2} - \frac{2\omega_L - f}{\Gamma^2 + (2\omega_L - f)^2} \right\} \right]. \end{aligned} \quad (15.52)$$

As the polarization angle α of the incident radiation is varied from 0 to $\pi/2$ the intensity of the resonant terms increases from zero to a maximum value. This corresponds to the change from π polarization when only the state $m=0$ is being excited, to σ polarization when atoms are excited to a coherent superposition of $m=\pm 1$ states. For $\alpha=\pi/2$ the expression given in equation (15.46) for the amplitude of the in-phase component of modulation is now easily verified, while the amplitude of the $\sin ft$ component of modulation is given by

$$B = \left\{ \frac{2f}{\Gamma^2 + f^2} - \frac{2\omega_L + f}{\Gamma^2 + (2\omega_L + f)^2} + \frac{2\omega_L - f}{\Gamma^2 + (2\omega_L - f)^2} \right\} I_0 \Gamma$$

and displays dispersion-shaped resonances at $2\omega_L = \pm f$. Further detailed studies of the resonance signals excited by modulated light are described by Corney (1968).

Problems

- 15.1. The Hanle effect is observed using the apparatus shown in Fig. 15.1. Prove that the polarization of the fluorescent light, defined by $P = (I_y - I_x)/(I_y + I_x)$, is given by $P = f^2 / (\Gamma^2 + 4\omega_L^2)$.

The geometry of the apparatus is then changed so that the magnetic field, the direction of the incident

light, and the axis of observation are mutually orthogonal; and the atoms are excited by unpolarized resonance radiation. Using the classical description of the Hanle effect show that the intensity of the fluorescent light observed without a polarizer is given by

$$I(B) = \frac{I_0 R}{2} \left\{ \frac{3}{\Gamma} - \frac{\Gamma}{\Gamma^2 + 4\omega_L^2} \right\}.$$

- 15.2. The widths of the Hanle signals, ΔB , observed in mercury vapour at low densities using the 1850 \AA and 2537 \AA resonance lines are found to have the values $85.1 \pm 5.26 \text{ G}$ and $0.649 \pm 0.011 \text{ G}$ respectively. The Landé g-factors for the 6^1P_1 and 6^3P_1 levels have the values 1.02 and 1.486 respectively. Calculate the radiative lifetimes of these levels and the absorption oscillator strengths of the corresponding resonance lines.

(Ans: $\tau(^1P_1) = (1.31 \pm 0.08) \times 10^{-9} \text{ s}$; $f_{ik} = 1.18$
 $\tau(^3P_1) = (1.18 \pm 0.02) \times 10^{-7} \text{ s}$; $f_{ik} = 0.0245$.)

- 15.3. The density matrix of an ensemble of spin $\frac{1}{2}$ particles in the $|m_s\rangle$ representation is given by

$$\rho = \begin{pmatrix} 1/2 & 0 \\ 0 & 1/2 \end{pmatrix}.$$

Using the spin angular momentum operators

$$s_x = \begin{pmatrix} 0 & 1 \\ 1 & 0 \end{pmatrix}, \quad s_y = \begin{pmatrix} 0 & -1 \\ 1 & 0 \end{pmatrix}, \quad s_z = \begin{pmatrix} 1 & 0 \\ 0 & -1 \end{pmatrix}$$

show that $\langle s_x \rangle = \langle s_y \rangle = \langle s_z \rangle = 0$.

In another experiment every particle of the ensemble is prepared in a coherent superposition of the $m_s = \pm \frac{1}{2}$ states such that

$$\rho = \begin{pmatrix} 3/4 & 1/4 \\ 1/4 & 1/4 \end{pmatrix}.$$

Show now that $\langle s_x \rangle = \langle s_z \rangle = \frac{1}{2}$ and $\langle s_y \rangle = 0$.

15.4. Show that the intensity of light of polarization \hat{e}' emitted as an atom in the Zeeman sub-level $|m\rangle$ decays radiatively to the sub-level $|\mu'\rangle$ of the ground state is given by equation (15.25).

15.5. The polarization vector \hat{e} shown in Fig. 15.10 is expressed in terms of the unit vectors $(\hat{i}, \hat{j}, \hat{k})$ by $\hat{e} = \hat{i} \cos\alpha + \hat{j} \sin\alpha$. Using the relationships which exist between the unit vectors $(\hat{i}, \hat{j}, \hat{k})$ and $(\hat{x}, \hat{y}, \hat{z})$ show that \hat{e} may also be expressed in the form given by equation (15.29). Hence complete the detailed derivation of the excitation matrix, equation (15.33).

15.6. The Hanle effect geometry of Fig. 15.1 corresponds to the case $(\theta=\pi/2, \phi=0, \alpha=\pi/2)$ and $(\theta'=0, \phi'=\pi/2)$. By substitution in equations (15.30) and equations (15.35)-(15.37), show that the intensity of the fluorescent light observed in this experiment for the case $J_e=1 \leftrightarrow J_g=0$ is given by

$$\frac{dI}{d\Omega} = \frac{C}{2\Gamma} \left\{ \frac{1}{\Gamma} + \frac{2\Gamma \cos 2\alpha'}{\Gamma^2 + 4\omega_L^2} + \frac{4\omega_L \sin 2\alpha'}{\Gamma^2 + 4\omega_L^2} \right\}.$$

15.7. The quantum theory of the Hanle effect predicts that the intensity of the fluorescent light is determined by the factor C/Γ , where

$$C = \frac{U(\omega)}{8\pi\varepsilon_0^2} \left(\frac{\omega}{hc} \right)^3 \langle D \rangle^4 \rho_{00}.$$

Hence show that when this fluorescent light is detected by a photomultiplier, the rate Q at which photoelectrons are released from the cathode surface is given by equation (15.38).

Calculate Q assuming the following values for the relevant parameters:

Total flux of resonance radiation incident on the cell	$= 10^{15}$ photons $\text{cm}^{-2} \text{s}^{-1}$
Illuminated area of resonance cell	$= 3 \text{ cm}^2$

Length of resonance cell	$= 2 \text{ cm}$
Density of ground state atoms in cell	$= 10^{10} \text{ cm}^{-3}$
Combined collection and cathode quantum-efficiency factor	$= 5 \times 10^{-5}$
Absorption oscillator strength of resonance line	$= 1 \times 10^{-3}$
Doppler width of both source and absorption cell	$= 1500 \text{ MHz}$
(Ans: 1.1×10^8 .)	

15.8. In a time-resolved experiment a sample of cadmium atoms is excited to the 5^3P_1 level by a short pulse of linearly polarized resonance radiation. The atoms are subjected to an external magnetic field of 0.345 G and the exponential decay of the fluorescent light is observed to be intensity modulated. Calculate the modulation frequencies expected for atoms of both the even ($I=0$) and the odd ($I=1/2$) isotopes of cadmium. (Ans: $\omega/2\pi = 1.45 \text{ MHz}; 0.724 \text{ MHz.}$)

15.9. The geometry of a pulsed resonance fluorescence experiment is described by the angles $(\theta=\pi/2, \phi=0, \alpha=\pi/2)$ and $(\theta'=\pi/2, \phi'=\pi/2)$. Using expressions similar to those developed in section 15.2.3, show that the intensity of the fluorescent light observed is given by

$$\frac{dI}{d\Omega} = \frac{C}{2} [1 - \cos(2\omega_L(t-t_0))] \exp[-\Gamma(t-t_0)].$$

15.10. A sample of gas at low pressure in zero magnetic field is subjected to a periodic excitation process, $R(t)$, which has a fundamental angular frequency ω . By expanding $R(t)$ as a Fourier series show that the intensity of light emitted by atoms or molecules in the excited level k is modulated and that the signal at the fundamental frequency is given by

$$S_\omega = S_0 \cos(\omega t - \phi_1)$$

where $S_0 = CA_{ki}((a_1^2 + b_1^2)/(\omega^2 + \Gamma^2))^{1/2}$ and $\phi_1 = \tan^{-1}(\omega/\Gamma)$.

The spontaneous transition probability of the observed line is A_{ki} and $\Gamma = 1/\tau_k$ is the effective total decay rate of the excited level k ; a_1 and b_1 are the in-phase and quadrature Fourier expansion coefficients of $R(t)$ at the fundamental frequency and C is an arbitrary constant. In such an experiment the phase shift ϕ_1 observed on the $A^1\pi \rightarrow X^1\Sigma$ transition of $N0^+$ is 62° at the fundamental frequency $\omega/2\pi = 5.5$ MHz. Calculate the effective lifetime of the excited $A^1\pi$ state.

(Ans: $\tau_k = 5.4 \times 10^{-8}$ s.)

References

- Aleksandrov, E.B. (1963). *Optics Spectrosc.* 14, 233.
 _____ (1964). *Optics Spectrosc.* 17, 522.
- Barrat, J.P. (1959). *J.Phys.,Paris* 20, 657.
 _____ and Butaux, J. (1961). *C.r.hebd.Séanc.Acad.Sci., Paris* 253, 2668.
- Brossel, J. and Kastler, A. (1949). *C.r.hebd.Séanc.Acad.Sci., Paris* 229, 1213.
- Byron, F.W.Jr., McDermott, M.N., and Novick, R. (1964a). *Phys.Rev.* 134, A615.
 _____, _____, _____ Perry, B.W., and Saloman, E.B. (1964b). *Phys.Rev.* 134, A47.
- Capelle, G., Sakurai, K., and Broida, H.P. (1971). *J.Chem.Phys.* 54, 1728.
- Carrington, C.G. (1972). *J.Phys.B.* 5, 1572.
 _____ and Corney, A. (1971). *J.Phys.B.* 4, 849.
- Corney, A. (1968). *J.Phys.B.* 1, 458.

- Corney, A. and Series, G.W. (1964a). *Proc.phys.Soc.,Lond.* 83, 207.
 _____ and _____ (1964b). *Proc.phys.Soc.,Lond.* 85, 213.
- Dodd, J.N., Kaul, R.D., and Warrington, D.M. (1964). *Proc.Phys.Soc.,Lond.* 84, 176.
- _____, Sandle, W.J., and Zisserman, D. (1967). *Proc.Phys.Soc.,Lond.* 92, 497.
- Erdmann, T.A., Figger, H., and Walther, H. (1972). *Opt.Comm.* 6, 166.
- Faure, A., Nedelec, O., and Pebay-Peyroula, J.C. (1963). *C.r.hebd.Séanc.Acad.Sci.,Paris* 256, 5088.
- Gallagher, A. (1967). *Phys.Rev.* 157, 24.
- Gornik, W., Kaiser, D., Lange, W., Luther, J. and Schultz, H.-H. (1972). *Opt.Comm.* 6, 327.
 _____, _____, _____, Luther, J., Meier, K., Radloff, H.-H., and Schultz, H.-H. (1973). *Phys.Lett.* 45A, 219.
- Hanle, W. (1924). *Z. Phys.* 30, 93.
- Harries, W.L. and von Engel, A. (1954). *Proc.R.Soc.* A222, 490.
- Kastler, A. (1950). *J.Phys.,Paris* 11, 255.
- Kibble, B.P. and Series, G.W. (1961). *Proc.Phys.Soc.,Lond.* 78, 70.
- Lombardi, M. and Pebay-Peyroula, J.C. (1965). *C.r.hebd.Séanc.Acad.Sci.,Paris* 261, 1485.
- Lurio, A. (1965). *Phys.Rev.* 140, A1505.
- Lurio, A. and Novick, R. (1964). *Phys.Rev.* 134, A608.
- Lurio, A., de Zafra, R.L., and Goschen, R.J. (1964). *Phys.Rev.* 134, A1198.
- Nedelec, O. (1966). *J.Phys.,Paris* 27, 660.

- Pebay-Peyroula, J.C. (1969). *Physics of the one- and two-electron atoms.* (Eds. F. Bopp and H. Kleinpoppen) p. 348. North-Holland, Amsterdam.
- Rayleigh, Lord (1922). *Proc.R.Soc.* 102, 190.
- Sakurai, K. and Capelle, G. (1970). *J.chem.Phys.* 53, 3764.
- _____, _____ and Broida, H.P. (1971). *J.chem.Phys.* 54, 1220.
- Schenck, P., Hilborn, R.C., and Metcalf, H. (1973). *Phys. Rev.Lett.* 31, 189.
- Schmieder, R.W., Lurio, A., and Happer, W. (1968). *Phys.Rev.* 173, 76.
- _____, _____, _____ and Khadjavi, A. (1970). *Phys.Rev.* A2, 1216.
- Wood, R.W. (1913). *Researches in physical optics*, Vols. I and II. Columbia University Press, New York.
- _____, Ellett, A. (1924). *Phys.Rev.* 24, 243.
- Wright, J.J., Dawson, J.F., and Balling, L.C. (1974). *Phys.Rev.* A9, 83.

General references and further reading

A wealth of information about early experiments on resonance fluorescence is contained in two text-books

Mitchell, A.C.G. and Zemansky, M.W. (1966). *Resonance radiation and excited atoms.* Cambridge University Press, London.

Wood, R.W. (1934). *Physical optics.* Macmillan, New York.

A clear account of the theory of the interaction of atoms and radiation has recently been published by

Loudon, R. (1973). *The quantum theory of light.* Clarendon Press, Oxford.

The theory of the density matrix is reviewed in an article by

Fano, U. (1957). *Rev.Mod.Phys.* 29, 74.

and the theoretical description of resonance fluorescence experiments in terms of the density matrix is developed in articles by

Barrat, J.P. and Cohen-Tannoudji, C. (1961). *J.Phys.,Paris.* 22, 329 and 443.

and

Cohen-Tannoudji, C. (1962). *Annls.Phys.* 7, 423 and 469.

The physical phenomena associated with the Hertzian coherence of the density matrix are discussed by

Novikov, L.N., Pokazan'ev, V.G. and Skrotskii, G.V. (1970). *Soviet Phys.Usp.* 13, 384.

_____, Skrotskii, G.V., and Solomakho, G.I. (1974). *Soviet Phys.Usp.* 17, 542.

ATOMIC AND LASER SPECTROSCOPY

16.4. Radiation trapping and coherence narrowing

16.4.1. Experimental measurements using linearly polarized light. The first detailed investigation of the width of optical double-resonance signals over a wide range of pressure were made by Guiochon *et al.* (1957). Both the odd and even isotopes of mercury were studied and similar measurements using the Hanle effect were made by Barrat (1957). These experiments demonstrated a pronounced narrowing of the resonance fluorescence signals as the mercury vapour pressure is increased. This leads to an increase in the value of τ_{eff} deduced from the widths of the measured signals, and results obtained by the two techniques for the even isotope ^{202}Hg are shown in Fig. 16.7. There is good agreement between the values of τ_{eff} obtained and further results are included in a review of the experimental data prepared by Barrat (1959a).

This narrowing of the signals is attributed to re-

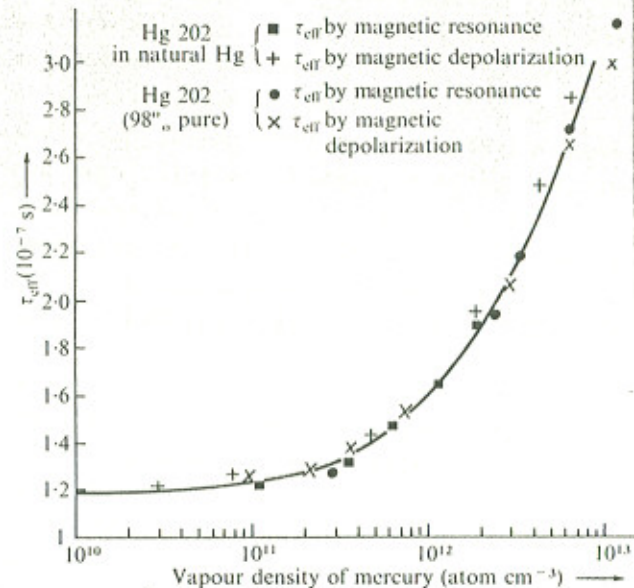


Fig. 16.7. Coherence narrowing of Hanle effect and optical double-resonance signals in ^{202}Hg at high vapour densities. (After Barrat (1957).)

absorption or trapping of the emitted resonance fluorescence photons within the cell. If the atoms which are involved in the multiple scattering process are contained in the same magnetic field, then the time development of their excited state wavefunctions will be identical. Consequently information about the polarization of the atom in the excited state can be partially transferred by a photon from one atom to another. The second atom can contribute to the observed signal and the lifetime of the atom has effectively been doubled. The resulting increase in the average lifetime of the ensemble of excited atoms causes the resonance signals to be narrower than expected and the phenomenon is therefore often called *coherence narrowing*.

Barrat (1959b) developed a density matrix theory to

describe the effect of this multiple scattering of resonance radiation, which was later improved by D'yakanov and Perel (1965a). For the moment we restrict ourselves to a consideration of the $J_e=1 \leftrightarrow J_g=0$ case. The theory shows that the shapes of the resonance fluorescence signals are unchanged but that in experiments in which linearly polarized light is used to excite the atoms, the natural linewidth appearing in equations in this and the previous chapter should be replaced by the effective decay rate

$$\Gamma_{\text{eff}} = \Gamma(1 - \frac{7}{10}x). \quad (16.25)$$

In this equation x is the probability that a photon emitted in the resonance line will be re-absorbed before leaving the cell and is given in terms of the absorption coefficient at the line centre, κ_0 , by

$$x = 1 - \frac{1}{\sqrt{\pi}} \int_{-\infty}^{\infty} \exp(-\kappa_0 L \exp(-y^2)) \exp(-y^2) dy \quad (16.26)$$

where the length parameter L is of the order of the dimensions of the resonance cell. Theoretical curves obtained by evaluating equation (16.25) are in good agreement with the experimental results over the density range from $10^{10} - 2 \times 10^{13} \text{ cm}^{-3}$.

Unfortunately it is difficult to extend these measurements to higher densities because strong multiple scattering is accompanied by a considerable depolarization of the fluorescent light and a consequential reduction in the signal-to-noise ratio. In the limit of very high densities, where the atoms are being isotropically irradiated by scattered photons, the fluorescent light is expected to be completely depolarized. Expressions for the percentage polarization at intermediate densities were obtained by Barrat (1959b) by averaging the coherence transferred over the arbitrary directions of propagation of the intermediate photons. For the case of excitation by linearly polarized light in the presence of a strong static field, the results are

$$\frac{P_\sigma}{100} = \frac{1-x}{1-3x/5}; \quad \frac{P_\pi}{100} = \frac{1-x}{1-4x/5} \quad (16.27)$$

for excitation by σ - and π -polarized light respectively. The r.f. magnetic field is assumed to be zero. The polarizations for both σ and π excitation and the amplitude of the Hanle effect signals all tend to zero at high densities, $x \approx 1$, as expected.

16.4.2. Comparison with delayed-coincidence lifetime measurements. It is interesting to note that the effective lifetimes measured by the resonance fluorescence techniques using linearly polarized light reach a theoretically predicted maximum value of $(10/3)\tau$ at high densities. This is in contrast to the lifetimes measured by the time-resolved techniques described in section 6.4 which increase indefinitely as trapping becomes more effective, as shown by Fig. 6.13. We must recognize that these two techniques are monitoring different parts of the ensemble density matrix. Those described in sections 6.3 and 6.4 measured only the rate of relaxation of the excited state population, determined by the diagonal elements of the excited state density matrix. On the other hand, the Hanle effect and optical double-resonance experiments using linearly polarized light measure a quantity called the *transverse alignment* which depends on the off-diagonal elements of ρ_e .

16.4.3. Experimental measurements using circularly polarized light. Further investigations of coherence narrowing by Omont (1965a) using circularly polarized light showed that there was yet a third relaxation rate. This characterizes the decay of the orientation of the excited state, a quantity which is proportional to the magnetic moment of the ensemble of excited atoms. The terms population, orientation, and alignment are explained in more detail in section 16.8. For the moment they can be identified approximately with the $\Delta m=0, 1$ and 2 terms respectively of the general expression for the Hanle effect signal given by equations (15.35)-(15.37).

The theoretical expression, equation (16.25), for the effective decay rate must now be cast in the more general form

$$\Gamma_{\text{eff}}^{(k)} = \Gamma \{1 - \alpha^{(k)}_x\}. \quad (16.28)$$

For the $J_e=1 + J_g=0$ case, the parameter $\alpha^{(k)}$ takes the following values:

Population	; k=0	$\alpha^{(0)}=1$
Orientation	; k=1	$\alpha^{(1)}=1/2$
Alignment	; k=2	$\alpha^{(2)}=7/10$

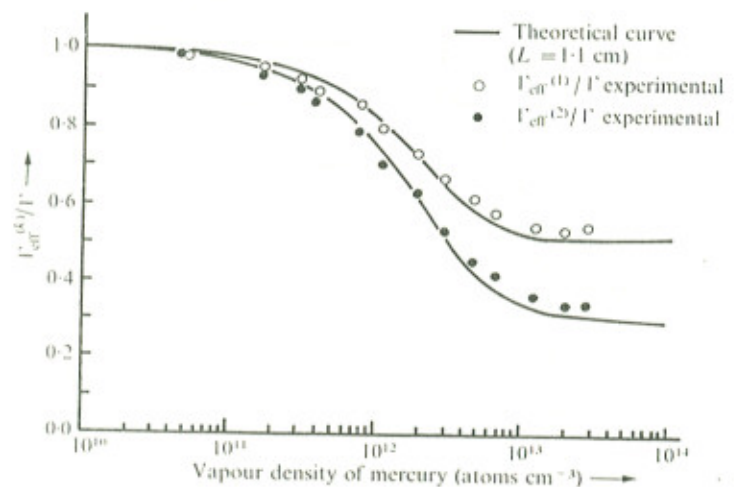


Fig. 16.8. Effect of radiation trapping on the relaxation rates of the orientation ($\Gamma^{(1)}$) and alignment ($\Gamma^{(2)}$) of a sample of ^{198}Hg atoms. The alignment lifetime is increased by a factor of 10/3 in the limit of complete trapping while the orientation lifetime is increased by a factor of 2. \circ , \bullet , experimental points; solid lines, theoretical curves. (After Omont (1965a).)

By using circularly and linearly polarized light alternatively in the same geometry, Omont (1965a) was able to measure both $\Gamma_{\text{eff}}^{(1)}$ and $\Gamma_{\text{eff}}^{(2)}$ using the Hanle effect in isotopically pure ^{198}Hg . The results obtained are plotted in Fig. 16.8 together with theoretical curves derived from equations (16.26) and (16.28) using $L=1.1$ cm. The agreement between the theory and experiment is obviously very good. The ratio of the orientation and alignment linewidths was checked by plotting $\{\Gamma - \Gamma_{\text{eff}}^{(1)}\}/\Gamma$ against $\{\Gamma - \Gamma_{\text{eff}}^{(2)}\}/\Gamma$ and an excellent fit to a straight line with a slope of 5/7 was obtained in complete agreement with the theory.

It was then realized that these different decay rates can be measured directly in delayed-coincidence experiments if suitably polarized light is used. Time-resolved experiments by Dodd *et al.* (1970) and also by Deech and Baylis (1971), which are similar to those described in section 15.8, have confirmed the original measurements made by Omont.

16.5. Collision broadening in resonance fluorescence experiments

16.5.1. Introduction. When Hanle effect or optical double-resonance experiments are extended to very high atomic densities, the width of the signal increases very rapidly. This is illustrated in Fig. 16.9 for the case of the Hanle signals from the $(6s^2 6p7s) \ ^3P_1$ level of lead studied by Happer and Saloman (1967). In the density range $10^{10}-10^{14} \text{ cm}^{-3}$ coherence narrowing is important, but above 10^{14} cm^{-3} there is a broadening of the signal due to collisions between the radiating excited atoms and other atoms in the electronic ground state. During a collision we can imagine that a torque is exerted on the classical oscillating dipole moment of the atom and that its direction of oscillation is changed. In terms of a fixed laboratory axis of quantization, this rotation can be described by a mixing of the different Zeeman sub-levels of the excited atom. Thus collisions cause the components of the ensemble-averaged density matrix

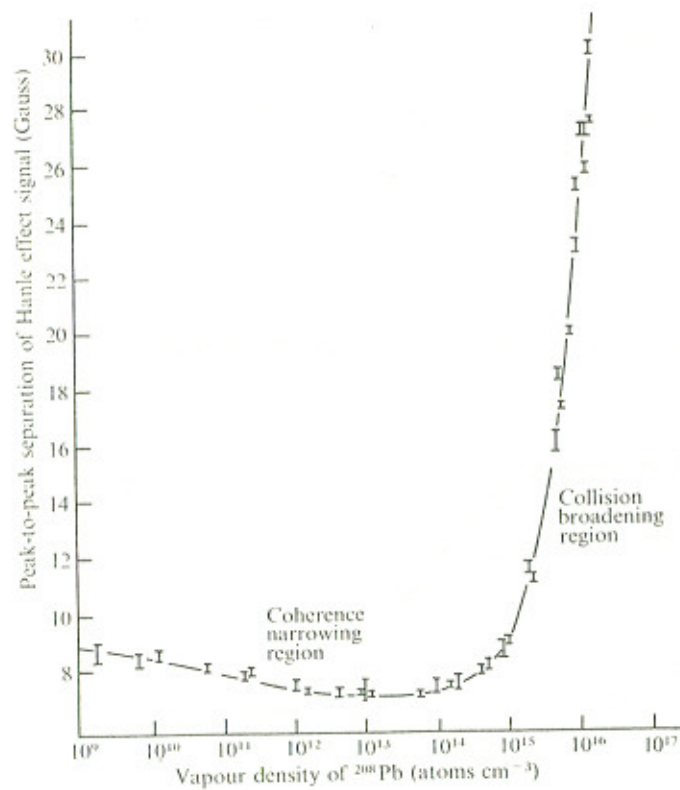


Fig. 16.9. Coherence narrowing and collision broadening of the width of the Hanle effect signals on the $^3\text{P}_1^0$ state of lead. (After Happer and Saloman (1967).)

to relax more quickly, leading to an increase in the widths of resonance fluorescence signals and to a reduction in the polarization of the fluorescent light observed in zero magnetic field.

As in the case of radiation trapping, collisions also cause the population, orientation, and alignment of the excited state to relax at different rates, the orientation being typically from 5 per cent to 25 per cent more sensitive

to collisions than the alignment. In many cases, however, collisional quenching of the excited atoms is negligible and the population relaxation rate is determined solely by the radiative lifetime. Long range electrostatic interactions are responsible for most of the collisional de-polarization and Hanle effect studies have become one of the most sensitive probes of this interaction. These experiments have recently stimulated considerable improvements in the theory of collision broadening.

The density range over which most resonance fluorescence experiments can be performed is such that only collisions involving two atoms need be considered. In this case the additional collisional relaxation rate, $r_{\text{coll}}^{(k)}$, may be expressed in terms of a binary collision cross-section $\sigma^{(k)}(v)$, averaged over the distribution of relative velocities v of the perturber and excited atoms:

$$r_{\text{coll}}^{(k)} = N(v \sigma^{(k)}(v))_{\text{Ave}}$$

where N is the number density of perturbers. It is usual to write this equation in terms of a velocity averaged cross-section, $\bar{v} \sigma^{(k)}(\bar{v})$, by assuming a Maxwellian distribution for the relative velocities, giving

$$\bar{v} \sigma^{(k)}(\bar{v}) = N \bar{v} \sigma^{(k)}(\bar{v}) \quad (16.29)$$

where

$$\bar{v} \sigma^{(k)}(\bar{v}) = (v \sigma^{(k)}(v))_{\text{Ave}}$$

and

$$\bar{v} = \left\{ \frac{8kT}{\pi} \frac{(M_1 + M_2)}{M_1 M_2} \right\}^{1/2}.$$

It is found that the effects of collision broadening and resonance trapping are additive, and the effective decay rate for the simple case of an excited atom which has only

a single allowed emission line becomes:

$$\Gamma_{\text{eff}}^{(k)} = \Gamma \{1 - \alpha_x^{(k)}\} + N\bar{v} \sigma^{(k)}(\bar{v}). \quad (16.30)$$

Thus in the region where binary collisions are dominant, the half-widths of the Hanle effect and optical double-resonance signals are proportional to the density of the perturbing atoms and these experiments provide an accurate means of measuring the velocity-averaged collision cross-sections. Although Mitchell and Zemansky (1966) include accounts of many early investigations of collision broadening, we shall not refer to these experiments again. The effects of resonance trapping, collisional quenching and of hyperfine structure were not sufficiently investigated by these early workers and an accurate interpretation of their measurements is now largely impossible.

16.5.2. Experimental investigations of resonance broadening.

The most important term in an expansion of the long-range interatomic potential is the electrostatic dipole-dipole interaction:

$$V(R) = -\frac{1}{4\pi\epsilon_0 R^3} \{3(\underline{D}_1 \cdot \hat{\underline{u}})(\underline{D}_2 \cdot \hat{\underline{u}}) - (\underline{D}_1 \cdot \underline{D}_2)\} \quad (16.31)$$

where $\underline{R} = \underline{R}_2 - \underline{R}_1$ is the position vector of the perturber (2) with respect to the excited atom (1) and $\underline{D}_a = -\sum_i e \underline{r}_i^a$ is the electric dipole operator for atom a. That part of equation (16.31) which is angular dependent is responsible for the collisional depolarization observed in resonance fluorescence experiments, while the scalar part is responsible for the broadening of the spectral distribution of the resonance line as discussed in section 8.2. When an excited atom in a resonance level collides with an identical atom in the ground state the odd parity operator of equation (16.31) possesses finite matrix elements in first-order perturbation theory (Problem 16.7). During the collision there is a resonant transfer of excitation from atom 1 to atom 2 and the depolarizing cross-sections can be as large as 10^{-12}

for strongly radiating states. These depolarization cross-sections are many hundreds of times larger than the gas kinetic cross-sections and are typical of resonance or self broadening collisions. As a first example we consider the resonance broadening of Hanle effect signals in lead.

(a) Resonance broadening of the $(6s^2 6p7s) \ ^3P_1^0$ level of lead. The $^3P_1^0$ level of lead may be excited from the ground state $(6s^2 6p^2) \ ^3P_0$ by absorption of resonance radiation at 2833 \AA , as shown in Fig. 16.10. Unlike mercury, the $6 \ ^3P_{1,0}$ level in lead can also decay by line fluorescence at 3639 \AA and 4058 \AA

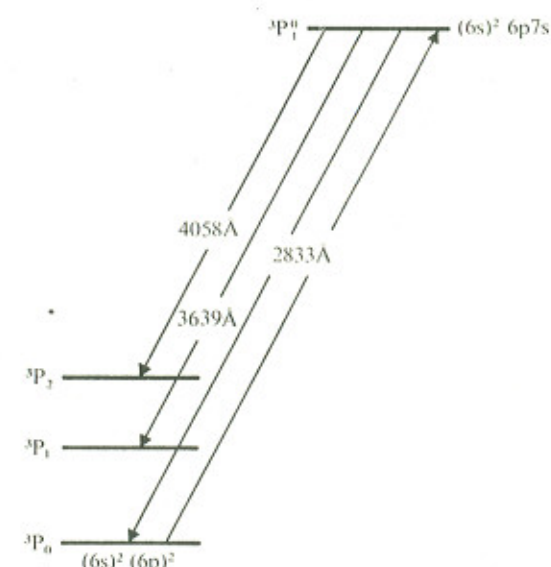


Fig. 16.10. Energy-level diagram showing the 3P_0 ground state of lead, the two metastable levels 3P_1 and 3P_2 , and the resonance level $^3P_1^0$. The thermal population of the metastable levels is normally very small so that little trapping of the cross fluorescent light at 4058 \AA and 3639 \AA occurs.

to the 3P_1 and 3P_2 levels. These metastable levels lie several tenths of an eV above the ground state and are not normally sufficiently populated to cause trapping of the 4058 \AA and 3639 \AA fluorescent light. Consequently the coherence narrowing and accompanying reduction in signal-to-noise due to depolarization are not nearly as great as they would have been in the absence of these branching transitions. This enabled Happer and Saloman (1967) to measure the depolarizing collision cross-sections using a fused quartz resonance cell containing a few milligrams of ^{208}Pb of 99.75 per cent purity. The results of their experiments are given in Table 16.2 and are discussed in more detail after the following section.

(b) Resonance broadening of the 6^3P_1 level of mercury. By contrast, in mercury at the high vapour pressures required for the observation of collision broadening, the polarization of the fluorescent radiation has become so weak owing to the depolarization caused by resonance trapping that the signal-to-noise ratio is too low for accurate measurements. The direct approach used by Happer and Saloman therefore fails. Fortunately the difficulty may be overcome by using a mixture of two isotopes. Thus if ^{202}Hg is present as a small concentration in a mixture with another isotope, such as ^{204}Hg , the resonance broadening cross-sections for the 6^3P_1 level of ^{202}Hg may be measured by illuminating the cell with resonance radiation from a lamp filled with ^{202}Hg . As Table 16.1 shows, the isotope shift is sufficiently large compared with the Doppler width of the 2537 \AA line that this radiation is not trapped by the ^{204}Hg which forms the main vapour in the cell. Nevertheless, since the isotopes have the same electronic structure, ^{204}Hg will depolarize ^{202}Hg on collision in exactly the same way that ^{202}Hg atoms would do, provided that the isotope shift $\Delta E \ll \hbar/T_c$ where T_c is the duration of one collision. This condition is satisfied by a number of different pairs of mercury isotopes.

With this technique Omont and Meunier (1968) were able

TABLE 16.1

Hyperfine structure of Hg 2537 \AA line

The positions of the components are measured with respect to that of the isotope ^{198}Hg

Isotope	Excited level quantum number	Position of component (10^{-3} cm^{-1}) F
201	1/2	+ 229.4
199	3/2	+ 224.6
198	1	0.0
201	3/2	- 22.6
200	1	- 160.4
202	1	- 337.2
201	5/2	- 489.3
204	1	- 511.1
199	1/2	- 514.3

to measure the cross-sections for the destruction of alignment and orientation of the 6^3P_1 level of mercury using the Hanle effect. Their results for ^{202}Hg broadened by ^{204}Hg are shown in Fig. 16.11. The non-linear variation of $\Gamma_{\text{eff}}^{(k)}$ as a function of density indicates that trapping of the fluorescence from ^{202}Hg has not been entirely eliminated. The measured values were therefore corrected by using equation (16.30) and choosing a concentration for the ^{202}Hg isotope such that the revised data were linear as a function of density. The cross-sections obtained in these experiments with different isotopic mixtures are in good agreement and only the average value is included in Table 16.2.

16.5.3. Comparison with theoretical calculations in resonance broadening. The impact theory of collision broadening in re-

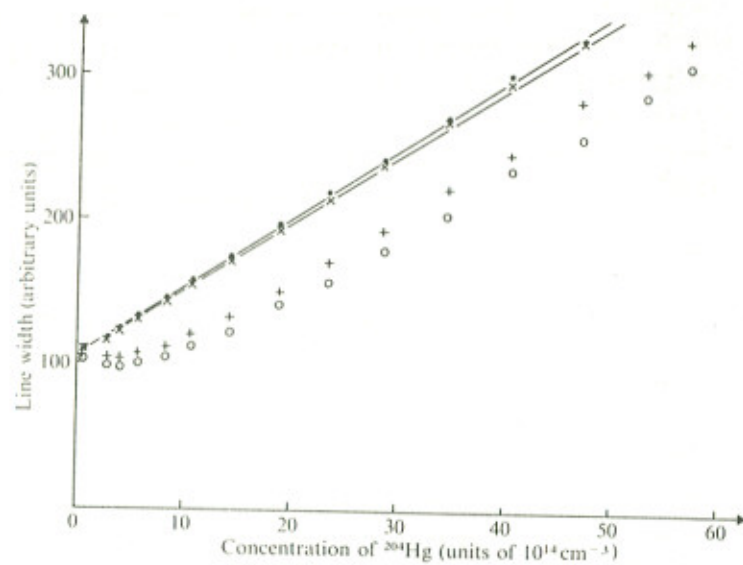


Fig. 16.11. Collision broadening of ^{202}Hg Hanle effect signals by ^{204}Hg atoms. Uncorrected measurements :
 o alignment; + orientation. Measurements corrected for radiation trapping assuming ^{202}Hg concentration as 2×10^{-3} : • alignment ; × orientation.
 (After Omont and Meunier (1968).)

sonance fluorescence experiments has been developed by Omont (1965b) and D'yakanov and Perel (1965b) using the density matrix approach. In the case of resonance broadening the theories predict that the collisional relaxation rate, $\Gamma_{\text{coll}}^{(k)}$, is independent of the relative velocities of the atoms and is proportional to the oscillator strength of the resonance line, $f_{J'J}$:

$$\Gamma_{\text{coll}}^{(k)} = \left\{ \frac{2\sqrt{3}}{3\pi} K^{(k)}(i) \right\} \frac{\pi e^2 f_{J'J} N}{8\varepsilon_0 m \omega_{J'J}} . \quad (16.32)$$

The constant $K^{(k)}(i)$ depends on the approximations made in the calculations and on the particular experimental method chosen to monitor a given multipole moment. The values of

TABLE 16.2

Resonance broadening collision cross-sections
in lead and mercury

Level studied	Orientation-destroying cross-section, $\sigma^{(1)}$ (10^{-13} cm^2)	Alignment-destroying cross-section, $\sigma^{(2)}$ (10^{-13} cm^2)	$\sigma^{(1)}/\sigma^{(2)}$
Pb($7s \ ^3P_1^0$) T=1240K	Experiment —	7.6 ± 1.7	1.21 ± 0.05
	Theory 7.50	6.25	1.20
Hg($6p \ ^3P_1$) T=350K	Experiment 1.38 ± 0.15	1.46 ± 0.15	0.95 ± 0.03
	Theory 1.45	1.51	0.96

$\kappa^{(k)}$ (i) shown in Table 16.3 were obtained in recent numerical solutions of the coupled differential equations appearing in the broadening theory and are expected to be accurate to between 1 per cent and 2 per cent. Using the f-values of the mercury and lead resonance lines obtained by experiments at low pressures, the theoretical broadening cross-sections determined from equations (16.29) and (16.32) have been evaluated and are given in Table 16.2. There is good agreement between the experimental and theoretical values of the cross-sections, and the agreement between the $\sigma^{(1)}/\sigma^{(2)}$ ratios, in which the experimental uncertainties in N and $f_{J,J'}$ are eliminated, is even more impressive. We can therefore be certain that the problem of depolarization in resonant collisions is now well understood.

TABLE 16.3

<i>Constants for collisional relaxation obtained by numerical integration in the resonance broadening case</i>		
Relaxation constant	Omont and Meunier (1968)	Carrington, Stacey and Cooper (1973)
$ee \kappa^{(1)}$ (1)	2.57	2.551
$ee \kappa^{(2)}$ (1)	2.72	2.652
$ee \kappa^{(2)}$ (1+2)	2.63	—

16.5.4. Experimental investigations of non-resonance

broadening. When the perturbing atoms or molecules are of a different chemical species from that of the emitter, the broadening is known as *foreign or non-resonance broadening*. In this case the dipole-dipole interaction of equation (16.31) has finite matrix elements only in second-order perturbation theory. The energy of interaction is propor-

tional to $1/R^6$ and is thus the angular equivalent of the scalar van der Waals potential discussed in section 8.2. This second-order calculation must also be used in the case of any level which does not possess an allowed electric dipole transition to the ground state. It also applies in cases such as the 4^3P_1 and 5^3P_1 levels of Zn and Cd respectively where the oscillator strength of the resonance line is very small. The resulting depolarization collision cross-sections are typically $10^{-15} - 10^{-14} \text{ cm}^2$, i.e. only slightly larger than the gas kinetic cross-sections. Indeed the cross-sections observed in foreign gas broadening are so small that the effects of the overlap of the wavefunctions of the emitter and perturber which give rise to short range repulsive forces often need to be considered.

(a) Foreign gas broadening of the 6^3P_1 level of mercury.

The depolarization of resonance fluorescence signals by foreign gases has been thoroughly investigated by Barrat et al. (1966) for the case of the 6^3P_1 level of ^{202}Hg . In the presence of collisions it can be shown that the polarization of resonance fluorescence excited by π -polarized light, equation (16.27), is modified to

$$\frac{P_\pi}{100} = \frac{\Gamma(1-x) + \Gamma_{\text{coll}}^{(0)}}{\Gamma(1-4x/5) + (\Gamma_{\text{coll}}^{(0)} + \Gamma_{\text{coll}}^{(2)})}. \quad (16.33)$$

For constant mercury vapour pressure the probability of photon re-absorption, x, is constant. Thus if the collisional quenching is negligible, $\Gamma_{\text{coll}}^{(0)} \approx 0$, a plot of $1/P_\pi$ is a linear function of the pressure of the perturbing gas, as shown in Fig. 16.12 for the noble gases and N_2 . From these graphs the alignment destruction cross-section, $\sigma^{(2)}$, can be obtained directly. Similar plots for the cases of depolarization by O_2 , H_2 , CO , and CO_2 showed definite curvature and values of $\sigma^{(0)}$ and $\sigma^{(2)}$ were obtained by manipulating equation (16.33) into a more suitable form. The values of the sums of the cross-sections, $(\sigma^{(0)} + \sigma^{(2)})$, were checked

by independent measurements of the widths of the Hanle effect signals excited by linearly polarized light, while observations with circularly polarized radiation enabled the sum of the quenching and orientation cross-sections, ($\sigma(0) + \sigma(1)$), to be obtained. The results of these measurements are given in Table 16.4. There is good agreement between the results obtained by the different techniques. It was found that quenching was absent in collisions with the noble gases and very small in the case of N₂. This corresponds to the fact that the electronic states of these perturbers are separated by several eV from the 6 3P₁ level of mercury. For quenching to take place all the electronic energy of the mercury atom would have to be converted into kinetic energy, which is a very unlikely process in two-body collisions.

TABLE 16.4

Collision cross-sections for foreign gas broadening of the 6 3P₁ level of mercury

Perturber	Polarization measurements		Hanle effect measurements	
	$\sigma(0)$ (10^{-16} cm ²)	$\sigma(2)$ (10^{-16} cm ²)	$\sigma(0) + \sigma(2)$ (10^{-16} cm ²)	$\sigma(0) + \sigma(1)$ (10^{-16} cm ²)
He	0	40.2	39.6	45.5
Ne	0	46.5	47.1	59.7
Ar	0	83.3	83.3	101
Kr	0	123	124	145
Xe	0	170	173	179
H ₂	25.1	33.0	56.6	61.3
N ₂	35	135	145	145
O ₂	62.8	53.4	112	112
CO	20.4	140	160	160
CO ₂	15.7	248	270	270

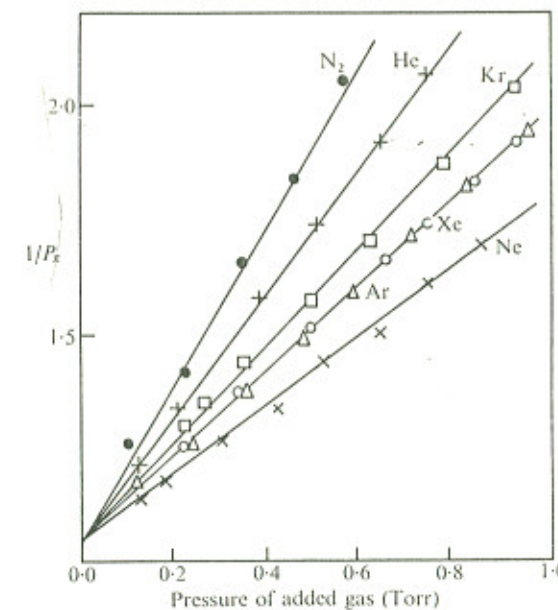


Fig. 16.12. Variation of (mercury resonance fluorescence polarization, P)⁻¹ as a function of the pressure of perturbing gas. (After Barrat *et al.* (1966).)

